Nucleic Acid Helix Stability: Effects of Salt Concentration, Cation Valence and Size, and Chain Length

Zhi-Jie Tan and Shi-Jie Chen
Department of Physics and Astronomy and Department of Biochemistry, University of Missouri, Columbia, Missouri 65211

ABSTRACT   Metal ions play crucial roles in thermal stability and folding kinetics of nucleic acids. For ions (especially multivalent ions) in the close vicinity of nucleic acid surface, interion correlations and ion-binding mode fluctuations may be important. Poisson-Boltzmann theory ignores these effects whereas the recently developed tightly bound ion (TBI) theory explicitly accounts for these effects. Extensive experimental data demonstrate that the TBI theory gives improved predictions for multivalent ions (e.g., Mg^{2+}) than the Poisson-Boltzmann theory. In this study, we use the TBI theory to investigate how the metal ions affect the folding stability of B-DNA helices. We quantitatively evaluate the effects of ion concentration, ion size and valence, and helix length on the helix stability. Moreover, we derive practically useful analytical formulas for the thermodynamic parameters as functions of finite helix length, ion type, and ion concentration. We find that the helix stability is additive for high ion concentration and long helix and nonadditive for low ion concentration and short helix. All these results are tested against and supported by extensive experimental data.

INTRODUCTION

Nucleic acid molecules are highly charged polyanion. In the folding of nucleic acids, the cations, such as sodium and magnesium ions, are required to neutralize the negative charges on the backbones to reduce the repulsive Coulombic interactions between the phosphates, so that the nucleic acid molecules can fold into the compact native structures. Ionic properties, such as ion concentration, charge, and size, play important roles in determining the stability and folding kinetics of nucleic acids (1–16).

Helices, which are formed by a train of consecutive basepairs, constitute the most important components in nucleic acid structures. Much effort has been devoted to the study of the helix stability. Most experimental measurements for the helix thermal stability are for the 1 M Na^+ salt condition (16–23). Our understanding of the helix stability under other ion conditions, especially in multivalent ion conditions, is quite limited (24–32). For example, previous studies examined the Na^+ or K^+-dependence of the helix melting temperature (22,33–35), and the folding free energy for DNA helix formation was extrapolated from the standard 1 M Na^+ condition to other Na^+ concentration ($\geq$0.1 M) (22). These empirically fitted extrapolations were mainly focused on the NaCl solution, not for the Mg^{2+} or other multivalent ion solutions (36–39). On the other hand, extensive experiments have demonstrated the essential role of Mg^{2+} in nucleic acids (3–5,10–14). For example, Mg^{2+} ions are found to be much more effective than Na^+ ions in stabilizing the DNA and RNA helices (36–39). Motivated by the desire to understand quantitatively the role of Mg^{2+} and other ions in the stabilization of DNA and RNA helices (40), we investigate the folding stability of DNA helix of finite length in the Mg^{2+} solution.

There have been two successful polyelectrolyte theories: the counterion condensation (CC) theory (41–43) and the Poisson-Boltzmann (PB) theory (44–51). The CC theory assumes a two-state ion distribution, and assumes a mean uniform distribution of condensed ions along the polyelectrolyte. In addition, the original CC theory is a double-limit law, i.e., it is for dilute salt solution and for nucleic acids of infinite length (41,52–54). The PB theory is a mean-field theory and ignores the interion correlation, which can be important for multivalent ions (e.g., Mg^{2+}). Recently, to treat the correlations and fluctuations for bound ions, we developed a tightly bound ion (TBI) model (55). The basic idea of the model is to separate the tightly bound ions from the diffusive ions in solution. The model explicitly accounts for the discrete modes of ion binding and the correlation between the tightly bound ions, and treat the bulk solvent ions using the PB. The model has been validated through extensive comparisons with Monte Carlo simulations. The TBI model agrees with PB and CC for Na^+ ions, of which the correlational effect is weak, and predicts improved results for Mg^{2+} (55), which can involve strong correlations.

In this study, the TBI theory is used to compute the helix-coil transition. The calculated results are validated through extensive tests against experiments. Based on the TBI model, we systematically investigate the thermodynamic stability of oligomeric DNA helices. We examine the dependence on the helix length and ion concentration for both NaCl and MgCl$_2$ solutions. In addition, we obtain an analytical expression for the folding stability parameters as a function of the ion concentration and the helix length for the NaCl and the MgCl$_2$ solutions.

THEORY

Thermodynamics

We model the helix as a double-stranded (ds) B-DNA helical structure and the coil as a single-stranded (ss) helical structure (see the ''Structural models for dsDNA and ssDNA'' section in Appendix A). The folding free energy (helix stability) ΔG_T° for the helix-coil transition is calculated as the difference between the helix and the coil:

$$\Delta G_T^\circ = G_T^\circ(\text{helix}) - G_T^\circ(\text{coil}). \qquad (1)$$

Here T is the temperature, $G_T^\circ(\text{helix})$ and $G_T^\circ(\text{coil})$ are the free energies for the helix and the coil, respectively. ΔG_T° is dependent on the temperature, the structures of the ds helix and the ss helix, and the solvent conditions, such as the salt concentration and the cation properties. As an approximation, we decompose ΔG_T° into two parts: a nonelectrostatic contribution ΔG_T^{nel} and an electrostatic contribution ΔG_T^{el} (32,33,56–60):

$$\Delta G_T^\circ = \Delta G_T^{\text{nel}} + \Delta G_T^{\text{el}}. \qquad (2)$$

ΔG_T^{nel}, which can be called the nonelectrostatic or ''chemical'' part of folding free energy, comes from the strong Watson-Crick basepairing and stacking interactions. We assume that ΔG_T^{nel} is salt-independent (32,33,56–60) and evaluate ΔG_T^{nel} using the nearest neighbor model with the measured thermodynamic parameters for the base stacks (17–23,61). Considering 1 M NaCl as the standard salt solution for the measurement of the nearest neighbor interaction parameters, we can calculate ΔG_T^{nel} by subtracting ΔG_T^{el} from the total folding free energy

$$\Delta G_T^{\text{nel}} = \Delta G_T^\circ(1\,\text{M Na}^+) - \Delta G_T^{\text{el}}(1\,\text{M Na}^+). \qquad (3)$$

Here the electrostatic free energy ΔG_T^{el} (1 M Na$^+$) can be calculated from the polyelectrolyte theory. The total free energy ΔG_T° (1 M Na$^+$) can be obtained from the nearest neighbor model using the experimentally measured thermodynamic parameters (17–23,61):

$$\Delta G_T^\circ(1\,\text{M Na}^+) = \sum_{\substack{\text{basestacks}}} (\Delta H^\circ(1\,\text{M Na}^+) - T\Delta S^\circ(1\,\text{M Na+})), \qquad (4)$$

where ΔH° (1 M Na$^+$) and ΔS° (1 M Na$^+$) are the enthalpy and entropy parameters for the base stacks in the helix at 1 M NaCl, respectively. As an approximation, we neglect ΔC_p, the heat capacity difference between helix and coil (62–68), so we can treat ΔH° (1 M Na$^+$) and ΔS° (1 M Na$^+$) as temperature-independent constants. Such approximation is valid if the temperature is not too far away from 37°C (22,64–68).

With ΔG_T^{el} calculated from the polyelectrolyte theory and ΔG_T^{nel} determined from Eq. 3, we can compute the folding free energy for any given NaCl or MgCl$_2$ concentration and temperature T:

$$\Delta G_T^\circ = \Delta G_T^{\text{nel}} + \Delta G_T^{\text{el}}(\text{Na}^+|\text{Mg}^{2+}) = \Delta G_T^\circ(1\,\text{M Na}^+)$$
$$+ [\Delta G_T^{\text{el}}(\text{Na}^+|\text{Mg}^{2+}) - \Delta G_T^{\text{el}}(1\,\text{M Na}^+)]. \qquad (5)$$

Here Na$^+$|Mg^{2+} denotes a pure NaCl or MgCl$_2$ solution.

For a given strand concentration C_S, the melting temperature T_m for helix-coil transition can also be obtained from the folding free energy ΔG_T° (22,68):

$$\Delta G_T^\circ - RT \ln C_S = 0 \quad \text{at} \quad T = T_m, \qquad (6)$$

where R is the gas constant (=1.987 cal/K/mol) and C_S is replaced by $C_S/4$ for non-self-complementary sequence.

Central to the calculation of the folding stability (free energy) is the computation of the electrostatic free energy ΔG_T^{el}. In this study, to account for the correlation and fluctuation effect for the bound ions, we use the recently developed TBI theory to compute ΔG_T^{el}. In the next section, we briefly summarize the TBI theory. Detailed discussion about the TBI theory can be found in Tan and Chen (55).

Summary of the tightly bound ion model

In the tightly bound ion (TBI) model, ions around a polyelectrolyte are classified into two types: the (strongly correlated) tightly bound ions and the (weakly correlated) diffusively bound ions, and the space around the nucleic acid can be correspondingly divided into the tightly bound region and the diffusively bound region, respectively. The rationale to distinguish the two types of ions (and the two types of spatial regions) is to treat them differently. For the diffusive ions, we can use PB. But for the tightly bound ions, we need a separate treatment to account for the correlations.

The strong correlation between the ions are characterized by the following two conditions:

a), Strong electrostatic correlation is characterized by a large Coulomb correlation parameter $\Gamma(\mathbf{r})$ at position $\mathbf{r}$:

$$\Gamma(\mathbf{r}) = \frac{(zq)^2}{\epsilon a_{\text{ws}}(\mathbf{r}) k_B T} \geq \Gamma_c, \qquad (7)$$

where $\Gamma(\mathbf{r})$ is the local correlation parameter, zq is the charge of the counterion (z is the valency of counterions and q is the proton charge), ϵ is the dielectric constant of the solvent, and $a_{\text{ws}}(\mathbf{r})$ is the Wigner-Seitz radius given by the cation concentration $c(\mathbf{r})$ in excess of the bulk concentration c^0 (69):

$$\frac{4\pi}{3}[a_{\text{ws}}(\mathbf{r})]^3[c(\mathbf{r}) - c^0] = 1. \qquad (8)$$

We choose Γ_c to be 2.6, the critical value for the gas-liquid transition to occur in an ionic system. Physically, for $\Gamma \geq \Gamma_c$, the Coulomb correlation is so strong that the charged system starts to exhibit liquid-like local order, whereas for $\Gamma < \Gamma_c$, the system is weakly correlated and is gaseous (70–72).

b), Strong excluded volume correlation is characterized by a small interion distance d

$$d = 2a_{\text{ws}} \leq 2(r_c + \Delta r), \qquad (9)$$

where r_c is the ion radius, Δr is the mean displacement of ions fluctuated from their equilibrium positions, and $2(a_{\text{ws}} - \Delta r)$ is the closest distance between two ions before they overlap. According to Lindemann's melting theory, we choose $\Delta r/d \simeq 0.1$ as the melting point for the correlated structure (73–75).

In the above analysis, we have implicitly assumed two types of distinguishable correlational effects: the ion-ion correlations that exist in bulk solvent (without the polyanionic nucleic acid) and the nucleic acid-induced correlations between the (bound) ions. The TBI model treats the second type correlational effects. Therefore, in the above equations, we use the excess ion concentration $c(\mathbf{r}) - c^0$ rather than the local concentration $c(\mathbf{r})$ in an attempt to account for the ''excess'' correlational effect induced by the nucleic acid for the bound ions. It is important to note that the use of the excess ion concentration is a rather crude approximation because, rigorously speaking, the above two types correlational effects are inseparable.

Ions that satisfy either of the above two correlation criteria (Eqs. 7 and 9) are classified as the tightly bound ions. The key to determine the tightly bound region is to obtain the ion concentration $c(\mathbf{r})$. As a crude approximation, we calculate $c(\mathbf{r})$ through the nonlinear PB equation

$$\nabla \cdot \epsilon_0 \epsilon \nabla \psi = -4\pi \left\{ \rho_f + \sum_\alpha z_\alpha q c_\alpha(\mathbf{r}) \right\}; \qquad (10)$$

$$c_\alpha(\mathbf{r}) = c_\alpha^0 e^{-z_\alpha q \psi(\mathbf{r})/k_B T}. \qquad (11)$$

Here, α denotes the ion species, $z_\alpha q$ is the charge of the ion, c_α^0 is the bulk ion concentration. ρ_f is the charge density of the fixed charges, ϵ_0 is the permittivity of free space, and $\psi(\mathbf{r})$ is the electrostatic potential at $\mathbf{r}$. We have developed a three-dimensional finite-difference algorithm to numerically solve nonlinear PB for $\psi(\mathbf{r})$ and $c(\mathbf{r})$ (55). From $c(\mathbf{r})$, the tightly bound region is quantitatively and unambiguously defined. In Fig. 1, we show
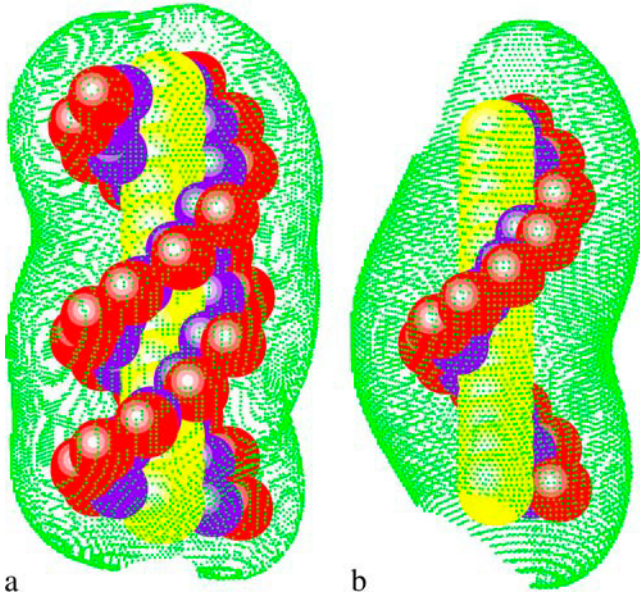
FIGURE 1 The tightly bound regions around (*a*) a 13-bp dsDNA and (*b*) a 13-nt ssDNA in Mg^{2+} solutions at bulk concentration $[MgCl_2] = 0.1$ M. The red spheres represent the phosphate groups and the green dots represent the points on the boundaries of the tightly bound regions. The dsDNA and ssDNA are produced from the grooved primitive model (see Appendix A) (55,95).

examples of the tightly bound regions around a ssDNA and a dsDNA helix in a Mg^{2+} solution.

For a *N*-bp double-stranded nucleic acid molecule, there are 2*N* phosphates. We divide the whole tightly bound region into 2*N* cells, each around a phosphate. In a cell, say, the *i*-th cell, there can exist $m_i = 0, 1, 2 \ldots$ tightly bound ions. Each possible set of the 2*N* numbers $\{m_1, m_2, \ldots, m_{2N}\}$ defines a binding mode. There exist a large number of such binding modes. For example, if we allow at most two ions in each cell, there would be 3^{2N} modes for the tightly bound ions. The total partition function *Z* is given by the sum over all the possible binding modes *M*:

$$Z = \sum_M Z_M, \tag{12}$$

where Z_M is the partition function for a given binding mode *M*.

How to compute Z_M for a given binding mode *M*? For a mode of N_b tightly bound ions and N_d diffusively bound ions, we use $\mathbf{R}_i$ ($i = 1, 2, \ldots, N_b$) and $\mathbf{r}_j$ ($j = 1, 2, \ldots, N_d$) to denote the coordinates of the *i*-th tightly bound ion and the *j*-th diffusive ion. The total interaction energy $U(\mathbf{R}, \mathbf{r})$ of the system for a given ion configuration $(\mathbf{R}, \mathbf{r}) = (\mathbf{R}_1, \mathbf{R}_2, \ldots, \mathbf{R}_{N_b}, \mathbf{r}_1, \mathbf{r}_2, \ldots, \mathbf{r}_{N_d})$ can be decomposed as three parts:

$$U(\mathbf{R}, \mathbf{r}) = U_b(\mathbf{R}) + U_{int}(\mathbf{R}, \mathbf{r}) + U_s(\mathbf{R}, \mathbf{r});$$

$U_b(\mathbf{R}) =$ the interaction between the charges
inside the tightly bound region (the tightly
bound ions and the phosphate charges);

$U_s(\mathbf{R}, \mathbf{r}) =$ the interaction between the diffusive ions;

$U_{int}(\mathbf{R}, \mathbf{r}) =$ the interaction between the diffusive ions and
the charges inside the tightly bound region.

Then, Z_M can be given by the following configurational integral (55)

$$Z_M = \frac{1}{(N_+ - N_b)!} \frac{1}{N_-!} \int_{V_R} \prod_{i=1}^{N_b} d\mathbf{R}_i \int_{V_r} \prod_{j=1}^{N_d} d\mathbf{r}_j e^{-U(\mathbf{R}, \mathbf{r})/k_B T}, \tag{13}$$

where N_+ and N_- are the total numbers of the cations and of the anions, respectively. In the above integral, for a given mode, $\mathbf{R}_i$ can distribute within the volume of the respective tightly bound cell whereas $\mathbf{r}_j$ can distribute in the volume of the bulk solution. V_R denotes the tightly bound region. The integration for $\mathbf{R}_i$ of the *i*-th tightly bound ion is over the respective tightly bound cell. V_r denotes the region for the diffusive ions. The integration for $\mathbf{r}_j$ of the *j*-th diffusive ion is over the entire volume of the bulk solvent. Averaging over the possible ion distributions gives the free energies ΔG_b and ΔG_d for the tightly bound and for the diffusive ions, respectively (55):

$$e^{-\Delta G_b/k_B T} = \langle e^{-U_b/k_B T} \rangle = \frac{\int \prod_{i=1}^{N_b} d\mathbf{R}_i e^{-U_b/k_B T}}{\int \prod_{i=1}^{N_b} d\mathbf{R}_i}; \tag{14}$$

$$e^{-\Delta G_d/k_B T} = \langle e^{-(U_{int} + U_s)/k_B T} \rangle = \int \prod_{j=1}^{N_d} \frac{d\mathbf{r}_j}{V} e^{-(U_{int} + U_s)/k_B T}. \tag{15}$$

Strictly speaking, for a given mode *M*, the free energy ΔG_d of diffusive ions is dependent on the spatial distribution $\mathbf{R}$ of the tightly bound ions in the tightly bound cells. However, assuming the dependence of ΔG_d on the tightly bound ions is mainly through the net tightly bound charge, which is fixed for a given mode, we can ignore the $\mathbf{R}$-dependence of ΔG_d. In practice, we approximate ΔG_d by $\Delta G_d(\overline{\mathbf{R}})$, where $\overline{\mathbf{R}}$ is the mean value of $\mathbf{R}$.

The decoupling of $\mathbf{R}$ and ΔG_d causes the separation of the $\mathbf{R}$ and the $\mathbf{r}$ variables in the configurational integral for Z_M, resulting in the following expression for Z_M (55):

$$Z_M = Z^{(id)} \left(\frac{N_+}{V} \right)^{N_b} \left(\int \prod_{i=1}^{N_b} d\mathbf{R}_i \right) e^{-\Delta G_b/k_B T} e^{-\Delta G_d/k_B T}. \tag{16}$$

Here, $Z^{(id)}$ is the partition function for the uniform solution without inserting the polyelectrolyte. The volume integral $\int \prod_{i=1}^{N_b} d\mathbf{R}_i$ provides a measure for the free accessible space for the N_b tightly bound ions. To obtain Z_M from Eq. 16, we need to calculate the free energies ΔG_b and ΔG_d.

To calculate ΔG_b, we note that the electrostatic interaction potential energy inside the tightly bound region U_b can be written as the sum of all the possible charge-charge interactions:

$$U_b = \sum_i u_{ii}(\mathbf{R}_i) + \sum_i \sum_j u_{ij}(\mathbf{R}_i, \mathbf{R}_j).$$

Here u_{ii} is the Coulomb interactions between the charges in cell *i* and u_{ij} is the Coulomb interactions between the charges in cell *i* and in cell *j*. We compute the potential of mean force $\Phi_1(i)$ for u_{ii} and $\Phi_2(i, j)$ for u_{ij}:

$$\Phi_1(i) = -k_B T \ln \langle e^{-u_{ii}(\mathbf{R}_i)/k_B T} \rangle;$$
$$\Phi_2(i, j) = -k_B T \ln \langle e^{-u_{ij}(\mathbf{R}_i, \mathbf{R}_j)/k_B T} \rangle. \tag{17}$$

Here, the averaging is over the possible positions $(\mathbf{R}_i, \mathbf{R}_j)$ of the tightly bound ion(s) in the respective tightly bound cell(s). From $\Phi_1(i)$ and $\Phi_2(i, j)$, we have

$$\Delta G_b \simeq \sum_i \Phi_1(i) + \sum_{ij} \Phi_2(i, j), \tag{18}$$

For ΔG_d, from the mean-field theory for the diffusive ions (76,77), we have (55):

$$\Delta G_{\mathrm{d}} = \frac{1}{2} \int \sum_{\alpha} c_{\alpha}(\mathbf{r}) z_{\alpha} e[\psi(\mathbf{r}) + \psi'(\mathbf{r})] d^3\mathbf{r}$$
$$+ k_{\mathrm{B}}\mathrm{T} \int \sum_{\alpha} \left[c_{\alpha}(\mathbf{r}) \ln\frac{c_{\alpha}(\mathbf{r})}{c_{\alpha}^0} - c_{\alpha}(\mathbf{r}) + c_{\alpha}^0 \right] d^3\mathbf{r}, \quad (19)$$

where the two integrals correspond to the enthalpic and entropic parts of the free energy, respectively. $\psi'(\mathbf{r})$ is the electrostatic potential for the system without the diffusive salt ions. $\psi'(\mathbf{r})$ is introduced because $\psi(\mathbf{r}) - \psi'(\mathbf{r})$ gives the contribution of the diffusive ions. $\psi(\mathbf{r})$ and $\psi'(\mathbf{r})$ are obtained from the nonlinear PB (Eq. 10) and the Poisson equation (without ions), respectively.

From the above equations, the electrostatic free energy can be computed as

$$G_{\mathrm{T}}^{\mathrm{el}} = -k_{\mathrm{B}}\mathrm{T} \ln(Z/Z^{(\mathrm{id})}) = -k_{\mathrm{B}}\mathrm{T} \ln \sum_{\mathrm{M}} (Z_{\mathrm{M}}/Z^{(\mathrm{id})}). \quad (20)$$

From Eq. 3 for the nonelectrostatic part ($\Delta G_{\mathrm{T}}^{\mathrm{nel}}$) and Eq. 20 for the electrostatic part ($\Delta G_{\mathrm{T}}^{\mathrm{el}}$), we can compute the free energy of a nucleic acid in the ds helix and the ss helix (coil) state, respectively. The free energy difference gives the stability of the ds helix structure, or, the folding free energy for the helix-coil transition.

In summary, the computation of the helix stability with the TBI theory involves the following steps (55):

First, for a polyanion molecule in salt solution, we solve the nonlinear PB (NLPB) to obtain the ion distribution $c(\mathbf{r})$ around the molecule, from which we determine the tightly bound region from Eqs. 7–9. In the nonlinear PB, we use dielectric constants $\epsilon = 2$ and 78 for the regions inside and outside the helix. We assign Debye-Huckel parameter $\kappa_{\mathrm{D}} = 0$ for the ion-inaccessible region for the ions (helix plus a charge-free layer with the thickness equal to the cation radius) and a nonzero κ_{D} determined by the ion concentration for the ion-accessible region (55).

Second, using Eq. 17, we compute the pairwise potential of mean force $\Phi_1(i)$ and $\Phi_2(i, j)$ for different cells (i and j's). Φ_1 and Φ_2 are calculated by averaging over all the possible positions of the tightly bound ions inside the respective tightly bound cells. The excluded volume effect is accounted for in the averaging (integration) process.

Third, we enumerate the possible binding modes. For each binding mode M: a), we solve the NLPB to obtain the distribution of the diffusive ions; b), from Eq. 19, we calculate the free energy for the diffusive ions and the interaction between the diffusive ions and the tightly bound ions ΔG_{d}; c), with the precalculated Φ_1 and Φ_2, we calculate the free energy of the tightly bound ions from Eq. 18; d), from Eq. 16, we compute the partition function Z_{M} for the mode.

Summing over the different binding modes gives the total partition function Z, from which we can calculate the free energy of the structure (ds or ss helix).

RESULTS

We investigate the ion-dependence of the folding thermo-dynamics for the helix-coil transition for a series of oligomeric DNAs of different lengths and sequences. In Table 1, we list the sequences, the thermodynamic parameters (ΔH°, ΔS°, ΔG°) in 1 M NaCl calculated from the nearest neighbor model, and the nonelectric part of the folding free energy $\Delta G_{\mathrm{T}}^{\mathrm{nel}}$ at $T = 37^\circ$C. To calculate $\Delta G_{\mathrm{T}}^{\mathrm{nel}}$, we calculate $\Delta G_{\mathrm{T}}^{\mathrm{el}}$ using the PB theory and the TBI model, respectively. From $\Delta G_{\mathrm{T}}^{\mathrm{el}}$, we obtain $\Delta G_{\mathrm{T}}^{\mathrm{nel}}$ from Eq. 3. In the following section, we will discuss the ion-dependence of the thermal stability of oligomeric DNA helices. Throughout the discussion, we focus on the comparisons with the available experimental data as well as with the results from the PB theory.

Salt concentration-dependence of the helix stability at 37°C

Electrostatic free energies G_{37}^{el} and $\Delta G_{37}^{\mathrm{el}}$

The electrostatic contribution to helix stability is quantified by the electrostatic folding free energy

$$\Delta G_{37}^{\mathrm{el}} = G_{37}^{\mathrm{el}}(\mathrm{helix}) - G_{37}^{\mathrm{el}}(\mathrm{coil}). \quad (21)$$

First, we calculate the electrostatic part of free energy G_{37}^{el} for the helix (dsDNA) and for the coil (ssDNA), respectively, as a function of the NaCl or MgCl$_2$ concentration. We show the results in Fig. 2, a and b, from which we make the following observations.

Higher ion concentration leads to lower electrostatic free energy G_{37}^{el}. This is because higher concentration corresponds to less entropy loss upon binding of the ion and thus enhances ion-binding. Moreover, the stabilization by higher ion concentration is more pronounced for ds helix than for ss helix (coil). As shown in Fig. 2, a and b, G_{37}^{el}(helix) of dsDNA decreases more rapidly than G_{37}^{el}(coil) of ssDNA (the *curves* of *black lines* are steeper than the ones of *gray lines* in the

TABLE 1 The DNA sequences used in the calculations

Sequence	N (bp)	Experiment reference	$-\Delta H^\circ$ (kcal/mol)*	$-\Delta S^\circ$ (cal/mol.K)*	$-\Delta G_{37}^\circ$ (kcal/mol)*	$-\Delta G_{37}^{\mathrm{nel}}$(PB) (kcal/mol)[†]	$-\Delta G_{37}^{\mathrm{nel}}$(TBI) (kcal/mol)[‡]
GCAGC	5	–	35.7	98.1	5.3	3.9	4.0
GCATGC	6	(36)	43.6	121.6	5.9	4.3	4.5
CCAAACA	7	(78)	46.8	130.8	6.2	4.2	4.5
GGAATTCC	8	(79–81)	55.2	156.0	6.8	4.5	4.8
GCCAGTTAA	9	(37)	63.1	174.8	8.9	6.3	6.7
ATCGTCTGGA	10	(35,82)	70.5	192.0	11.0	8.0	8.5
CCATTGCTACC	11	(35)	81.1	222.5	12.1	8.8	9.4
CAAAGATTCCTC	12	(83)	87.4	243.8	11.8	8.2	9.0
AGAAAGAGAAGA	12	(84,85)	83.1	231.2	11.4	7.8	8.6
CCAAAGATTCCTC	13	–	95.4	263.7	13.6	9.6	10.4

*The thermodynamic data are calculated at standard state (1 M NaCl) through the nearest-neighbor model with the thermodynamic parameters of SantaLucia (22).
[†]$\Delta G_{37}^{\mathrm{nel}}$(PB) is computed from Eq. 3 with $\Delta G_{37}^{\mathrm{el}}$ calculated from the Poisson-Boltzmann theory.
[‡]$\Delta G_{37}^{\mathrm{nel}}$(TBI) is calculated from Eq. 3 with $\Delta G_{37}^{\mathrm{el}}$ calculated through the tightly bound ion model. For each of the listed sequences, we have performed the thermodynamic calculations for both the NaCl and the MgCl$_2$ solutions of different ion concentrations.
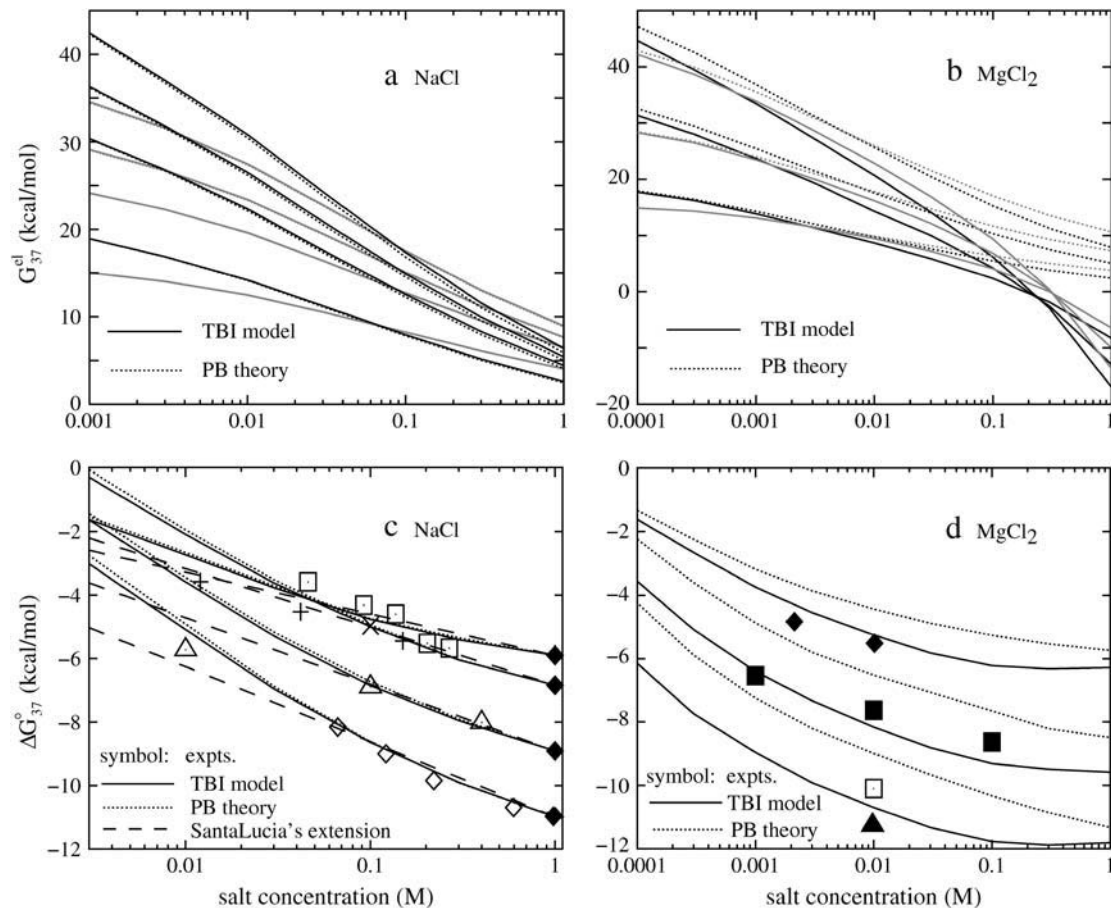
FIGURE 2 (a,b) The electrostatic free energy G_{37}^{el} for dsDNA (*black lines*) and the respective ssDNA (*gray lines*) as functions of (a) NaCl and (b) MgCl$_2$ concentrations. (*Dotted lines*) Poisson-Boltzmann theory; (*solid lines*) the TBI theory. (a) DNA length N are 10, 9, 8, and 6 bp (from the *top to bottom*), respectively; (b) DNA length N are 12, 9, and 6 bp (from the *top to bottom*), respectively. (c,d) The folding free energies ΔG_{37}° due to dsDNA helix formation for different sequences of various lengths in (c) NaCl and (d) MgCl$_2$ solutions. (*Dotted lines*) Poisson-Boltzmann theory; (*solid lines*) the TBI theory; (*dashed lines*) SantaLucia's salt extrapolation formula for NaCl (22,40). (c) The sequences used for NaCl solution are: GCATGC, GGAATTCC, GCCAGTTAA, and ATCGTCTGGA (from the *top to bottom*). The symbols are the experimental data. + GCATGC (36); □ GGAATTCC (79); × GGAATTCC (80); △ GCCAGTTAA (37); ◇ ATCGTCTGGA (82); ♦ are calculated from the nearest neighbor model with the thermodynamic parameters of SantaLucia at 1 M NaCl (22). (d) The sequences used for MgCl$_2$ are: GCATGC, GCCAGTTAA, and AGAAAGAGAAGA (from the *top to bottom*). The symbols are the experimental data: ■ GCCAGTTAA in MgCl$_2$ (37); □ AGAAAGAGAAGA in MgCl$_2$ (84); ▲ AGAAAGAGAAGA in MgCl$_2$ (85); ♦ GCATGC in NaCl/MgCl$_2$ mixed solution with 0.012 M NaCl (36). The experimental data in NaCl/MgCl$_2$ mixed solutions for GCATGC are used for semiquantitative comparison because NaCl is at very low concentration (36). For the MgCl$_2$ solutions, the values of ΔG_{37}^{nel}(TBI) from the TBI theory are used in the calculations of ΔG_{37}°.

figure). This is because dsDNA is more negatively charged than ssDNA (see Appendix A for the structures of the dsDNA and the ssDNA) and the stronger electrostatic effect leads to more pronounced increase of bound ions for higher salt concentration. As a result, higher salt concentration leads to a lower $\Delta G_{37}^{el} = G_{37}^{el}(\text{helix}) - G_{37}^{el}(\text{coil})$ (see Eq. 1), i.e., higher salt concentration tends to stabilize the helix.

From Fig. 2 a, we find that PB and TBI give nearly the same results for the NaCl solution. This is because the interion correlations are negligible for the NaCl solution considered here (55). However, for MgCl$_2$ solution, as shown in Fig. 2 b, we find that the TBI model gives lower free energy than the PB. This is because the low-energy correlated states of the bound Mg^{2+} ions, which are explicitly considered in TBI, are neglected in the PB. The average mean-field states

considered in PB have higher energies than the low-energy correlated states, causing the PB to underestimate the helix stability in the MgCl$_2$ solution.

Folding free energy ΔG_{37}°

Combining the electrostatic free energy G_{37}^{el} and the chemical free energy G_{37}^{nel}, we obtain the total free energy ΔG_{37}°(= the ds helix stability). We investigate the dependence of the helix stability as a function of the NaCl and the MgCl$_2$ concentrations for different DNA sequences and different helix lengths. Fig. 2, c and d, show our computed results as well as the experimental results.

As we expected, both Fig. 2, c and d, show that higher ion concentration supports higher helix stability (lower ΔG_{37}°).

This is because, as we discussed above, higher ion concentration gives lower electrostatic folding free energy ΔG_{37}^{el}.

In both the NaCl (Fig. 2 c) and the MgCl$_2$ (Fig. 2 d) solutions, longer helices have lower ΔG_{37}^{el} and thus are more stable than shorter ones. This is because longer helix means stronger attractive electric field for bound ions, and this effect is stronger for ds helix, which is more negatively charged, than for coil.

Besides the PB and TBI computational results, also plotted in Fig. 2 c for the NaCl solution are the experimental data and the results from SantaLucia's empirical extrapolated [Na$^+$]-dependence of ΔG_{37}° (22,40). As we discussed above, PB and TBI give the same results for NaCl solution. From Fig. 2 c, we find that, as tested against experiments, both theories give good results. Moreover, we find that SantaLucia's salt-dependence gives good results for [Na$^+$] between 0.1 and 1 M NaCl, and overestimates the helix stability for [Na$^+$] < 0.1 M.

Shown in Fig. 2 d is the MgCl$_2$ concentration-dependence of the electrostatic free energy ΔG_{37}° We find that both PB and TBI predict the same qualitative dependence of ΔG_{37}° in MgCl$_2$ concentration. However, compared with the experimental data for the three tested sequences GCATGC (36), GCCAGTTAA (37), and AGAAAGAGAAGA (84,85), TBI gives improved predictions than PB. As we discussed above, PB underestimates the helix stability owing to the neglected correlations between the bound Mg^{2+} ions. Fig. 2 d shows that the helix stability saturates at high MgCl$_2$ concentration (>0.03 M).

Temperature-dependence of helix stability

Temperature-dependence of the total stability ΔG_T°

We calculate the folding free energy ΔG_T° from Eq. 5 for NaCl and MgCl$_2$ solutions for different temperatures. We use the temperature-dependent dielectric constant of water in Eq. 33 (86). For both the Na$^+$ and Mg^{2+} salt solutions, as shown in Fig. 3, a and b, helix is more stable (i.e., is more negative $\Delta G_T^{\circ} = \Delta H^{\circ} - T\Delta S^{\circ}$) for lower temperatures. Also, we find that for all the tested sequences and ion concentrations, the TBI theory gives good predictions for the helix stability as tested against experiments. To understand the electrostatic contribution to the helix stability, we further investigate the temperature-dependence of the electrostatic part of the folding free energy ΔG_T^{el} (see Eq. 21).

Temperature-dependence of the electrostatic folding free energy ΔG_T^{el}

As shown in Fig. 4, in both the NaCl and the MgCl$_2$ solutions, the temperature-dependence of the electrostatic folding free energy ΔG_T^{el} is much weaker than that of the total free energy (net stability) ΔG_T°. So the strong temperature-dependence of helix stability predominantly comes from the temperature-dependence of the nonelectrostatic part ΔG_T^{nel}.
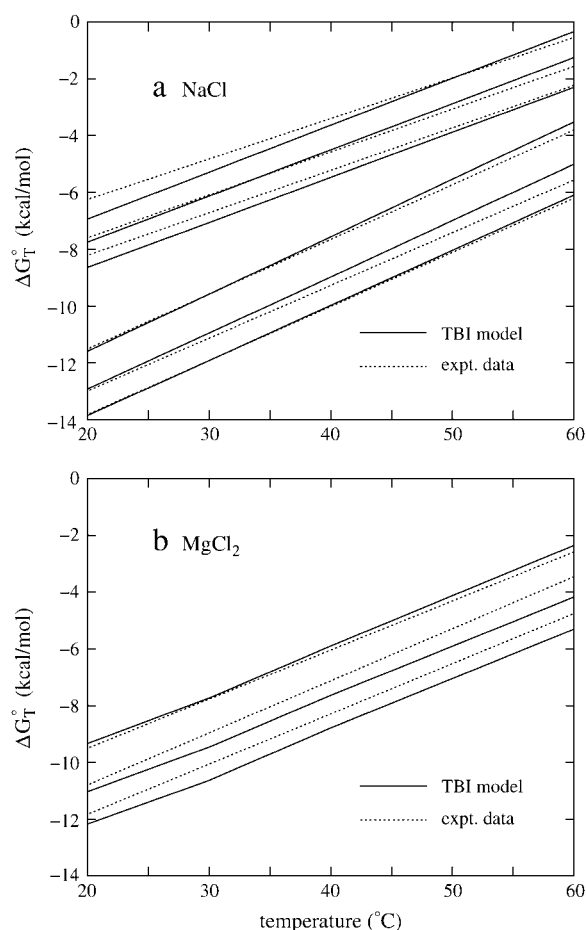

FIGURE 3   The temperature-dependence of the folding free energy ΔG_T° for (a) NaCl and (b) MgCl$_2$ solutions. (*Solid lines*) The TBI theory; (*dotted lines*) experimental data with the use of the equation $\Delta G_{T^{\circ}} = \Delta H^{\circ} - T\Delta S^{\circ}$, where ΔH° and ΔS° are taken from experiments. (a) The upper three lines are for sequence GGAATTCC at 0.046, 0.1, and 0.267 M NaCl (from the *top to bottom*) (79,80), and the bottom three lines are for sequence ATCGTCTGGA at 0.069, 0.22, and 0.62 M NaCl (from the *top to bottom*) (82). (b) The three lines are for sequence GCCAGTTAA at 1, 10, and 100 mM MgCl$_2$ (from the *top to bottom*) (37).

In the Na$^+$ salt solution. Plotted in Fig. 4 c is the temperature-dependence of ΔG_T^{el} for different NaCl concentrations for a 10-bp dsDNA. We find that ΔG_T^{el} is weakly dependent on temperature. As temperature is increased, ΔG_T^{el} decreases at high NaCl concentration and increases at low NaCl concentration. Such temperature-dependence is predicted by both PB and TBI. The temperature-dependence of electrostatic free energy can be understood from the temperature-dependence of the dielectric constant ϵ of the solvent (see Eq. 33): At higher temperature, ϵ is smaller, resulting in stronger Coulomb interactions. As explained below, the Coulomb interactions can be strengthened differently in dsDNA and ssDNA, resulting in the temperature-dependence of $\Delta G_T^{el} = \Delta G_T^{el}(ds) - \Delta G_T^{el}(ss)$.

For low [Na$^+$], ion binding is accompanied by a large entropic decrease and thus there are only few bound ions and
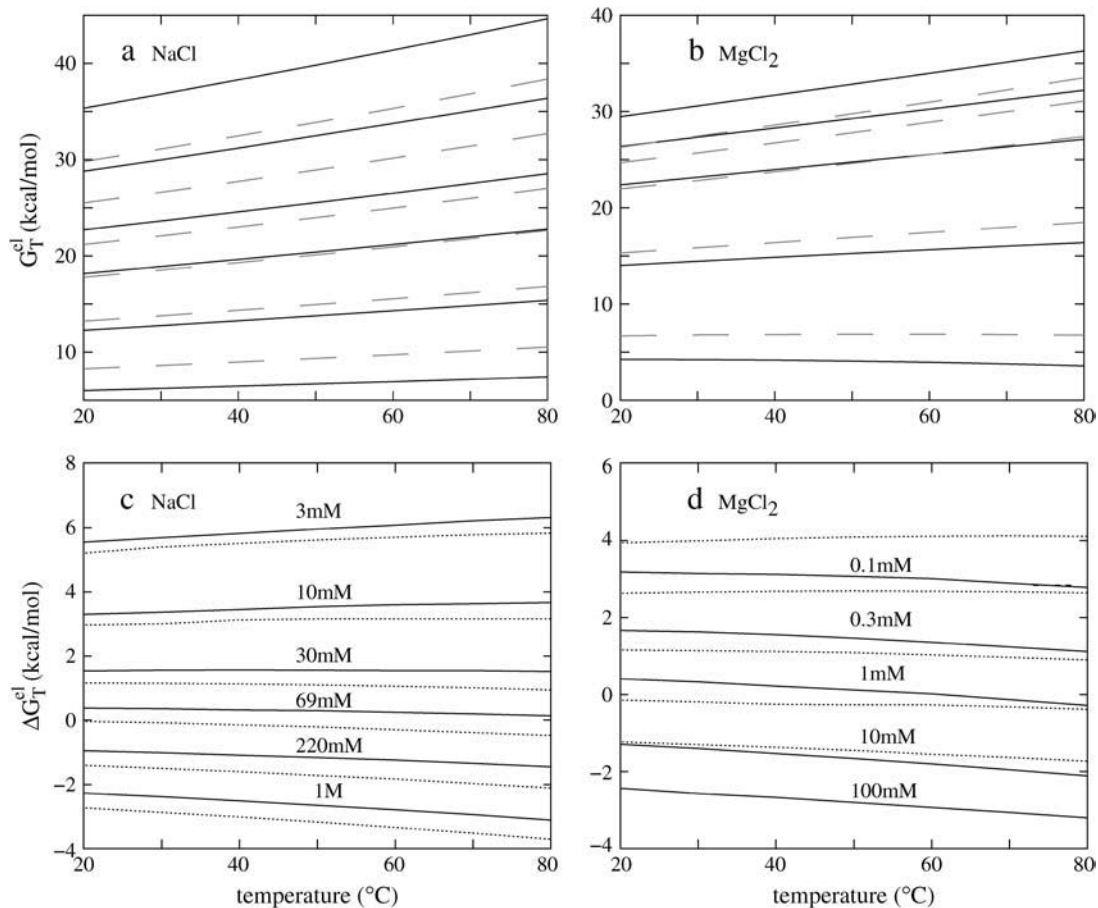
FIGURE 4 The temperature-dependence of the electrostatic part of the free energy. (*a,b*) The electrostatic free energy G_{37}^{el} of dsDNA (*solid lines*) and ssDNA (*dashed lines*) as functions of temperature: (*a*) for a 10-bp dsDNA and the respective ssDNA at 3 mM, 10 mM, 30 mM, 69 mM, 220 mM, and 1 M NaCl (from the *top to bottom*); (*b*) for a 9-bp dsDNA and the respective ssDNA at 0.1, 0.3, 1, 10, and 100 mM MgCl$_2$ (from the *top to bottom*). (*c,d*) The temperature-dependence of electrostatic contribution ΔG_{37}^{el} to folding free energy for dsDNA helix formation in (*c*) NaCl and (*d*) MgCl$_2$ solutions. (*Dotted lines*) Poisson-Boltzmann theory; (*solid lines*) the TBI theory. (*c*) Sequence ATCGTCTGGA at 3 mM, 10 mM, 30 mM, 69 mM, 220 mM, and 1 M NaCl (from the *top to bottom*); (*d*) sequence GCCAGTTAA at 0.1, 0.3, 1, 10, and 100 mM MgCl$_2$ (from the *top to bottom*).

weak charge neutralization. In such a case, the repulsive interactions between the phosphates dominate. dsDNA has higher phosphate charge density and thus the increase of the repulsive Coulomb interactions (due to the smaller ϵ at higher temperature) is stronger than ssDNA, causing an increase of ΔG_T^{el} as the temperature is increased.

For high NaCl concentration, more ions are bound, causing strong charge neutralization. Because the ds helix has much greater charge neutralization than ss helix (coil), as temperature is increased, the increase in the electrostatic interaction in ssDNA is more significant than in dsDNA (see Fig. 4 *a*), causing a decrease in ΔG_T^{el}.

In the Mg^{2+} salt solution. As shown in Fig. 4 *d* for a 9-bp dsDNA immersed in a MgCl$_2$ solution, ΔG_T^{el} decreases slightly with increasing temperature over a wide range of MgCl$_2$ concentration ($\gtrsim$0.1 mM MgCl$_2$). dsDNA has more bound ions and stronger charge neutralization than ssDNA, e.g., for 0.1 mM [MgCl$_2$], our TBI theory predicts that at

37°C, the tightly bound Mg^{2+} ions can neutralize 35% of the phosphate charge for a 9-bp dsDNA as compared to only 5% for the corresponding 9-nt ssDNA. So the Coulomb interaction in ssDNA is strengthened more significantly with the increase of temperature than that in dsDNA, resulting in a decrease in $\Delta G_T^{el} = G_T^{el}(ds) - G_T^{el}(ss)$ with the increase of temperature. The PB theory can predict the same trend but as we discussed above, PB underestimates the stability of ions because of the neglected correlation and fluctuation effects for the Mg^{2+} ions.

Salt-dependence of the melting temperature T_m

In the above section, we found that the predicted temperature-dependence of ΔG_T° from TBI agrees with the experiments for both the NaCl and the MgCl$_2$ solutions. Here, we calculate the melting temperature T_m (through Eq. 6) and compare the calculated results with the experimental data.
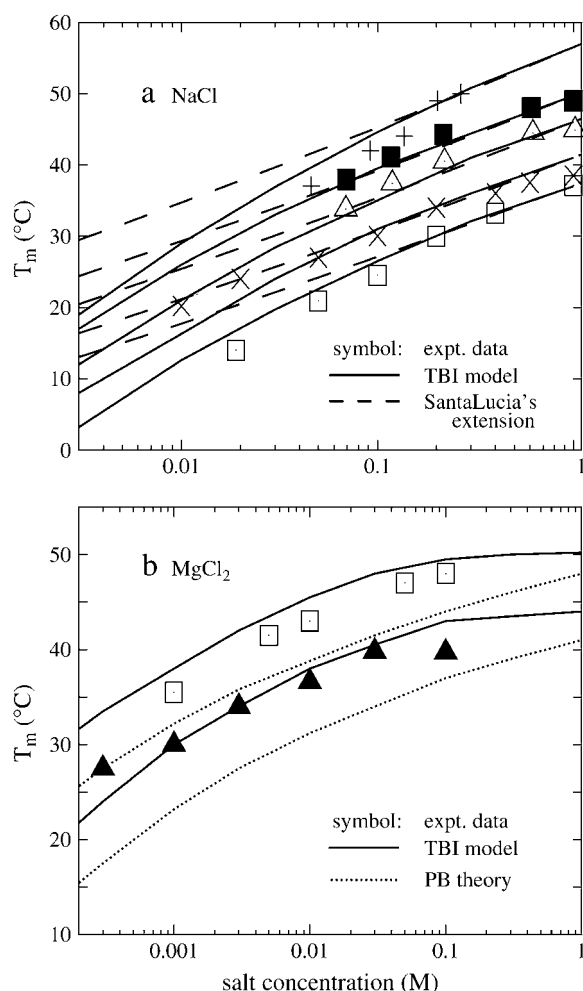
FIGURE 5   The melting temperature T_m for dsDNA of different sequences in (*a*) NaCl and (*b*) MgCl$_2$ solutions. (*Solid lines*) The TBI theory; (*dotted lines*) Poisson-Boltzmann theory; (*dashed lines*) SantaLucia's salt extension for NaCl (22,40); (*symbols*) the experimental data. (*a*) The sequences and total strand concentrations C_S are (from the *top to bottom*): + GGAATTCC at C_S = 3 mM (79); ■ CCATTGCTACC at C_S = 2 μM (35); △ ATCGTCTGGA at C_S = 2 μM (35); × GCCAGTTAA at C_S = 8 μM (37); and □ GGAATTCC at C_S = 18.8 μM (81). (*b*) The sequences and C_S are (from the *top to bottom*): □ AGAAAGAGAAGA at C_S = 6 μM (84); and ■ GCCAGTTAA at C_S = 8 μM (37). Here, the data for AGAAA-GAGAAGA are taken from the duplex melting in the study of the triplex melting in MgCl$_2$ and C_S = 6 μM is the total strand concentration for triplex formation. T_m is calculated from $\Delta G^\circ_T - RT\ln C_S/6 = 0$ (84).

In the NaCl solution

Shown in Fig. 5 *a* is the calculated melting temperatures T_m of dsDNA as functions of the NaCl concentration for different sequences and lengths. Also shown in the figure is the experimental data for the sequences GGAATTCC (79,80), GCCAGTTAA (37), ATCGTCTGGA (35), and CCATTGC-TACC (35). From the figure we find that the predicted T_m's are in agreement with the experimental results. The increase of the NaCl concentration leads to a higher T_m (higher stability of dsDNA helix). As a comparison, we also show SantaLucia's

empirical salt extension (fitted from experimental data) for the NaCl solution (22,40):

$$1/T_m = 1/T_m^\circ + 0.000368 \times (N - 1)\ln[Na^+]/\Delta H^\circ, \quad (22)$$

where T_m° and ΔH° are the melting temperature and the enthalpy change in 1 M NaCl solution. The above SantaLucia's empirical extension provides a good approximation for NaCl concentration between 0.1 and 1 M (22,40). We also calculate the T_m's for the experimental sequences GCATGC (36), CCAAACA (78), CAAAGATTCCTC (83). Again our calculated results agree with the experimental data.

In the MgCl$_2$ solution

Fig. 5 *b* shows the melting temperatures T_m of dsDNA helix in the MgCl$_2$ solution as a function of the ion concentration for two sequences. In contrast to the folding free energy ΔG_{37}° in Fig. 2 *d*, which has very limited experimental data, more experimental data for T_m in pure MgCl$_2$ solutions are available. We find that the T_m's predicted from the TBI model agree with the available experimental data over a wide MgCl$_2$ concentration range from 0.3 mM to 0.3 M. Again we find that PB theory can predict the trend in the [Mg^{2+}]-dependence of T_m but it underestimates the helix stability and the T_m due to the neglected correlation and fluctuation effects, as discussed in the previous sections.

Helix length-dependence of the electrostatic folding free energy ΔG_{37}^{el}

In this section, we investigate the dependence of ΔG_{37}^{el}, the electrostatic component of the helix stability, on the helix length. We use the number of basepairs N to define the helix length. We will also examine how the electrostatics affects the validity of the additive nearest neighbor model for the nucleic acid helix stability (17–23). To focus on the length-dependence and the additivity effect, we study the electro-static free energy ''per base stack'' $g_{37}^{el} = G_{37}^{el}/(N - 1)$ and $\Delta g_{37}^{el} = \Delta G_{37}^{el}/(N - 1)$.

Fig. 6, *a* and *b*, show the length-dependence of g_{37}^{el} for the dsDNA and the ssDNA. We find that for both ssDNA and dsDNA, g_{37}^{el} increases rapidly with N at low salt (NaCl or MgCl$_2$) concentrations and is only weakly dependent on N at high salt concentrations. The change in the length-dependence with the salt concentrations comes from the ion concentration-dependence of the charge neutralization (screening) effect. At low salt concentration, the neutraliza-tion is weak (the amount of bound ions is small), and the increase of helix length enhances the repulsive interactions between the charges (phosphate plus bound ion) in the backbone, causing an increased g_{37}^{el} with increased helix length (for both the ds- and the ss-helices). For high salt concentration, charge neutralization and ionic screening are strong (Debye length is short), so the increase in g_{37}^{el} is
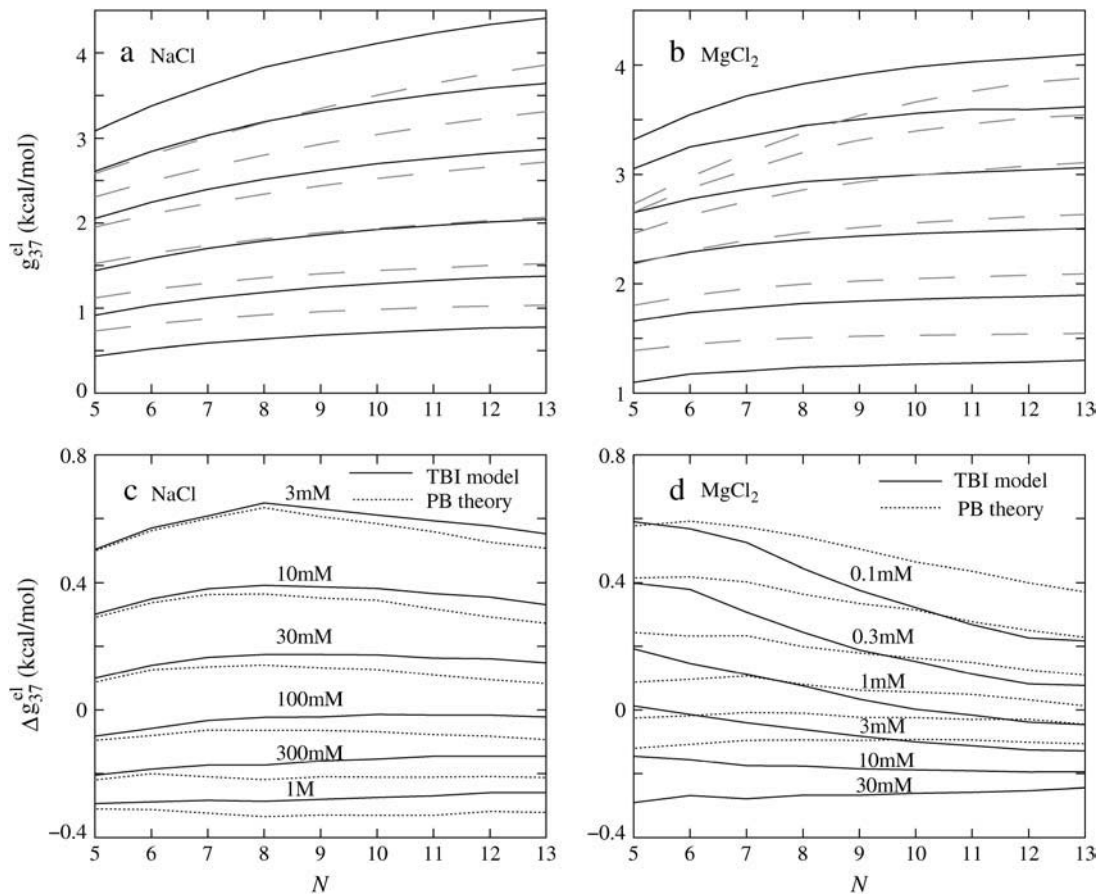
FIGURE 6 The length-dependence of the electrostatic part of the free energy. $g_{37}^{el} = G_{37}^{el}/(N-1)$ and $\Delta g_{37}^{el} = \Delta G_{37}^{el}/(N-1)$ are the electrostatic free energies per base stack. $N-1$ is the number of base stacks for a N-bp helix. (a,b) The electrostatic free energy g_{37}^{el} (per base stack) for dsDNA (*solid lines*) and the respective ssDNA (*dashed lines*) as functions of sequence length N in NaCl (a) and MgCl$_2$ (b) solutions. (a) [NaCl] = 3 mM, 10 mM, 30 mM, 100 mM, 300 mM, and 1 M (from the *top to bottom*); (b) [MgCl$_2$] = 0.1, 0.3, 1, 3, 10, and 30 mM (from the *top to bottom*). (c,d) The length N-dependence of electrostatic contribution $\Delta g_{37}^{el} = g_{37}^{el}(\text{dsDNA}) - g_{37}^{el}(\text{ssDNA})$ (per base stack) to folding free energy for dsDNA helix formation in NaCl (c) and MgCl$_2$ (d) solutions. (*Dotted lines*) Poisson-Boltzmann theory; (*solid lines*) the TBI theory. [NaCl] = 3 mM, 10 mM, 30 mM, 100 mM, 300 mM, and 1 M (from the *top to bottom*); [MgCl$_2$] = 0.1, 0.3, 1, 3, 10, and 30 mM (from the *top to bottom*).

retarded. As explained in the following, the difference between g_{37}^{el} of ssDNA and that of dsDNA determines electrostatic contribution to the helix stability per base stack $\Delta g_{37}^{el} = g_{37}^{el}(\text{ds}) - g_{37}^{el}(\text{ss})$.

In the NaCl solution

Shown in Fig. 6 c is the Δg_{37}^{el} calculated from both the PB theory and the TBI theory for different helix length N (-bp). As expected from the behavior of g_{37}^{el} in Fig. 6 a, Δg_{37}^{el} is weakly dependent on N for high NaCl concentration ($>$0.1 M).

For low NaCl concentration, the relationship between Δg_{37}^{el} and N becomes more complex: Δg_{37}^{el} increases with N when N is small, and decreases when N is large. Such nonmonotonic behavior can be explained as follows. At low NaCl concentration and for short DNA (small N), Na$^+$ ion binding is weak and the repulsive phosphate-phosphate repulsion dominates G_{37}^{el}. Due to the long-range nature of the

repulsive Coulomb interactions, G_{37}^{el} would increase nonlinearly with length N. Furthermore, such destabilizing effect is stronger for ds helix than for ss helix (coil). As a result, the ds helix is less stable than the ss helix. With the increase of N, the ds helix becomes increasingly less stable (i.e., an increasing Δg_{37}^{el}); see Fig. 6, a and c. If N continues to increase, the electric field near the negatively charged DNA surface will become stronger and will attract more bound Na$^+$ ions to neutralize the phosphate charges. This would retard the increase of the electrostatic free energy G_{37}^{el}, especially for the ds helix, which involves stronger electrostatic interactions. As a result, Δg_{37}^{el} decreases.

For high [NaCl], as shown in Fig. 6 c, Δg_{37}^{el} is approximately independent of N. So ΔG_{37}^{el} is additive for high NaCl concentrations (17–23). But for low NaCl, Δg_{37}^{el} is N-dependent. As a result, the additivity may fail.

Also shown in the figure is that PB and the TBI theory give nearly identical results for short DNA at low NaCl concentration. With the increase of DNA length and increase

of NaCl concentration, there exist very small differences between the two theories owing to the increased number of the (strongly correlated) ions in the tightly bound region. For example, for a 13-bp DNA at 1 M NaCl, the difference between the two theories is ~0.07 kcal/mol per base stack.

In the MgCl$_2$ solution

For the MgCl$_2$ solutions, the helix length N-dependence of Δg_{37}^{el} is shown in Fig. 6 d. For high MgCl$_2$ concentration, the dependence is rather weak due to the large charge neutralization. For low MgCl$_2$ concentration, ds helix is electrostatically unstable ($\Delta g_{37}^{el} > 0$), and Δg_{37}^{el} decreases rapidly with the increase of N when N is small, and become saturated when N is large. This is because as N is increased, the strong negative electric field near DNA surface causes an increased tendency of ion binding and charge neutralization, and such effect is stronger for ds helix than for ss helix, causing a decrease in Δg_{37}^{el}. When N becomes sufficiently large, both ds and ss helix can have strong charge neutralization, so the decrease of Δg_{37}^{el} with longer length would slow down (saturate). In addition, it can be seen that PB and TBI give similar results for short N and low MgCl$_2$ concentration because of the smaller number of bound ions and hence the weaker correlational effect. For large N and high [MgCl$_2$], more Mg^{2+} ions are bound near the DNA and these ions become strongly correlated. In such cases, the TBI model gives improved predictions (55).

Effect of the cation size on DNA stability

To investigate the effect of the cation size on the helix stability, we choose different radii for the (hydrated) monovalent and divalent cations. Specifically, we use 3, 3.5, and 4 Å for monovalent ions and 4, 4.5, and 5 Å for the divalent ions. Fig. 7 shows the folding free energy $\Delta G_{37}°$ as a function of ion concentration and ion size for sequence ATCGTCTGGA. We find that smaller cations support higher stability of dsDNA. We also find that different cation sizes give almost the same trend of the salt concentration-dependence of $\Delta G_{37}°$. Through experimental comparisons, we find that ion radius of 3.5 Å for Na$^+$ and 4.5 Å for Mg^{2+} can give the best fit for the experimental results for the helix stability and the melting temperature.

Small cations are more effective in stabilizing dsDNA because they can approach the phosphates and the grooves at a closer distance and can thus interact with DNA more strongly. Because dsDNA is more negatively charged than the corresponding ssDNA, the ion size-induced enhancement of the ion binding is stronger for dsDNA than for ssDNA. Thus, dsDNA becomes more stable in smaller cation solutions.

The predictions are in accordance with the experiments on dsDNA helix melting in various salt solutions (37). Recent experiments on RNA folding have also shown that smaller cations can stabilize RNA tertiary structure more effectively than larger ions (13). For more complex nucleic acid struc-
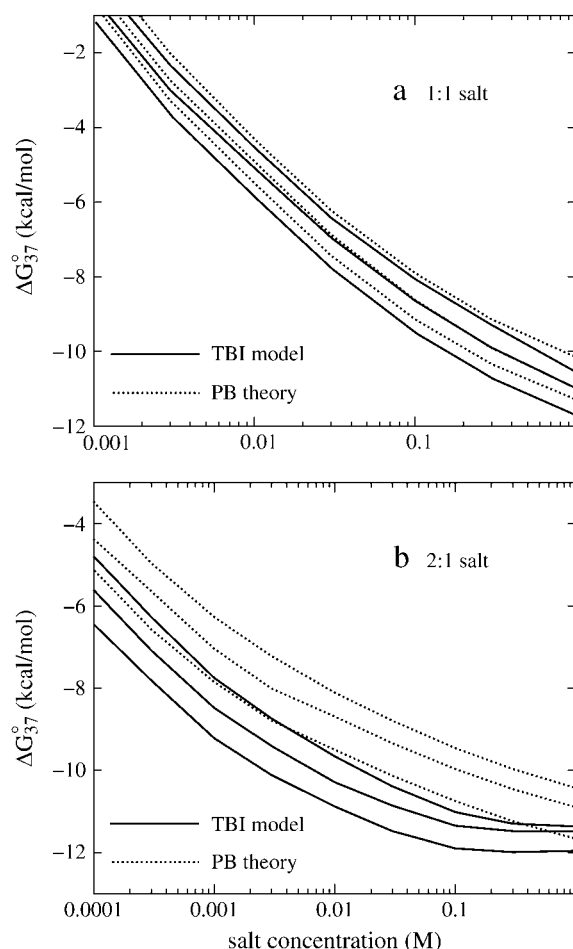

FIGURE 7 The folding free energies $\Delta G°_{37}$ for dsDNA helix formation as functions of (a) 1:1 and (b) 2:1 salt concentrations for sequence ATCGTCTGGA. (*Solid lines*) The TBI theory; (*dotted lines*) Poisson-Boltzmann theory. (a) The radii of monovalent cations are: 3, 3.5, and 4 Å (from the *bottom to top*). (b) The radii of divalent cations are: 4, 4.5, and 5 Å (from the *bottom to top*), respectively.

ture, the ion size can affect the ion-binding affinity through the compatibility with the geometry of binding site.

Thermodynamic parameters as functions of the ion concentration and the helix length

The availability of the (empirical) thermodynamic parameters for nucleic acids is limited by the availability of the experimental data. For example, for nucleic acids in NaCl solution, most experimental studies have been focused on high NaCl concentrations (e.g., 1 M), and thus the empirical salt-dependence fitted from the experiments are valid only for relatively high [Na$^+$] ($\gtrsim$0.1 M NaCl) (22,40). Moreover, there are very limited experimental data on the Mg^{2+}-dependence for different helix lengths. Therefore, it is desirable to have analytical formulas for the thermodynamic parameters as a function of [Na$^+$], [Mg^{2+}], and the helix length N (-bp). Such formulas would be practically valuable for thermodynamic

studies of nucleic acid stability. In this section, based on the TBI model and the comparisons with the available experimental data for DNA helix melting (22,32–35,40,87), we derive such empirical formulas.

NaCl solutions

By computing ΔG°_{37} for a wide range of DNA helix length and Na^+ concentrations using the TBI theory, we obtain the following (fitted) analytical expression for ΔG°_{37} as a function of $[Na^+]$ and N (number of basepairs in the helix):

$$\Delta G^\circ_{37}[Na^+] = \Delta G^\circ_{37}(1\,M) + (N-1)\Delta g_1. \qquad (23)$$

Here $(N-1)$ is the number of base stacks in the helix and Δg_1 is a function associated with the electrostatic folding free energy per base stack:
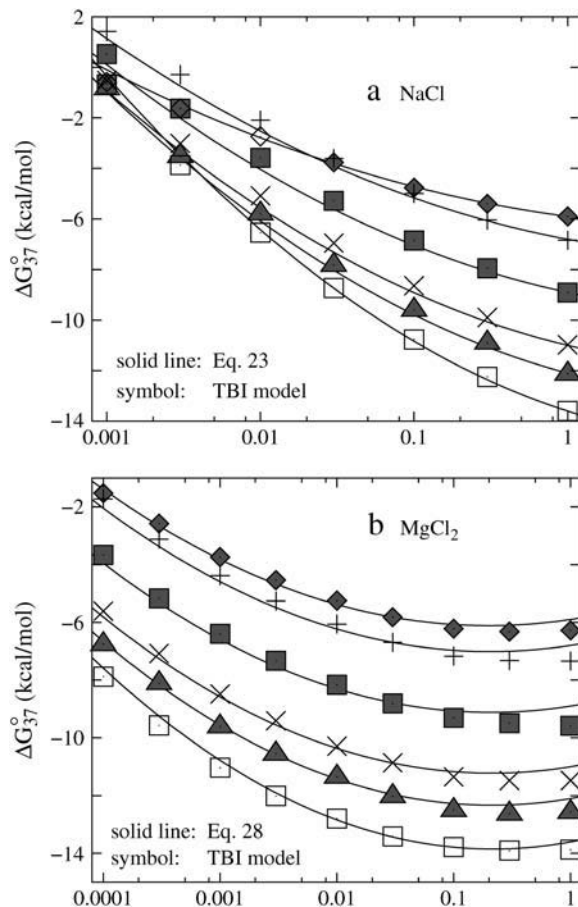
$$\Delta g_1 = a_1 + b_1/N; \qquad (24)$$

FIGURE 8   The free energy change ΔG°_{37} for dsDNA helix formation as functions of (*a*) NaCl and (*b*) MgCl$_2$ concentrations for the sequences: GCATGC, GGAATTCC, GCCAGTTAA, ATCGTCTGGA, CCATTGC-TACC, and CCAAAGATTCCTC (from the *top to bottom*). (*a*) (*Solid lines*) The empirical relation Eq. 23; (*symbols*) calculated from the TBI theory. (*b*) (*Solid lines*) The empirical relation Eq. 28; (*symbols*) calculated from the TBI theory.

$$a_1 \simeq -0.07\ln[Na^+] + 0.012\ln^2[Na^+];$$
$$b_1 \simeq 0.013\ln^2[Na^+]. \qquad (25)$$

The above empirical expression for the folding free energy gives good fit with the TBI results for NaCl concentration from 1 mM to 1 M (shown in Fig. 8 *a*). Assuming that the salt-dependence of ΔG°_T is mainly entropic, i.e., enthalpy change ΔH° is mainly independent of NaCl concentration (22,25,30,40,41), we obtain the following expression for the entropy change ΔS° (in cal/mol/K) for the helix $\rightarrow$ coil transition.

$$\Delta S^\circ[Na^+] = \Delta S^\circ(1\,M) - 3.22(N-1)\Delta g_1. \qquad (26)$$

From Eqs. 23 and 26, neglecting the temperature-dependence of the enthalpy and entropy parameters, we obtain the following expression for the folding free energy ΔG°_T for any given temperature T and Na^+ concentration: $\Delta G^\circ_T([Na^+]) = \Delta H^\circ(1\,M) - T\Delta S^\circ[Na^+]$, where $\Delta H^\circ(1\,M)$ and $\Delta S^\circ(1\,M)$ can both be calculated from the nearest neighbor model with the use of the measured thermodynamic parameters (17–22,40,61).

Furthermore, from Eqs. 23 and 26, we obtain the following empirical expression for the melting temperature T_m:

$$1/T_m[Na^+] = 1/T^\circ_m(1\,M) - 0.00322(N-1)\Delta g_1/\Delta H^\circ(1\,M). \qquad (27)$$

As shown in Fig. 9 *a*, the above expression for T_m agrees with the experimental results, even for very long DNA (*Escherichia coli*) (33).

In the MgCl$_2$ solution

Similarly, from Eqs. 3 and 5, we obtain the following expression for the thermodynamic parameters in MgCl$_2$ solution:

$$\Delta G^\circ_{37}[Mg^{2+}] = \Delta G^\circ_{37}(1\,M) + (N-1)\Delta g_2; \qquad (28)$$
$$\Delta S^\circ[Mg^{2+}] = \Delta S^\circ(1\,M) - 3.22(N-1)\Delta g_2; \qquad (29)$$
$$1/T_m[Mg^{2+}] = 1/T^\circ_m(1\,M) - 0.00322(N-1)\Delta g_2/\Delta H^\circ(1\,M), \qquad (30)$$

where Δg_2 is a function associated to the electrostatic folding free energy per base stack, Δg_2 is a function of helix length N and the Mg^{2+} ion concentration:

$$\Delta g_2 = a_2 + b_2/N^2; \qquad (31)$$
$$a_2 = 0.02\ln[Mg^{2+}] + 0.0068\ln^2[Mg^{2+}];$$
$$b_2 = 1.18\ln[Mg^{2+}] + 0.344\ln^2[Mg^{2+}]. \qquad (32)$$

The above analytical expressions are valid for $N \gtrsim 6$ (see Fig. 8 *b* for the comparison with the TBI calculations). Fig. 9 *b* shows the comparison between the above formulas and the experimental data for T_m for a wide range of Mg^{2+} concentration and DNA length. We find good agreements between Eq. 30 and the available experimental data.
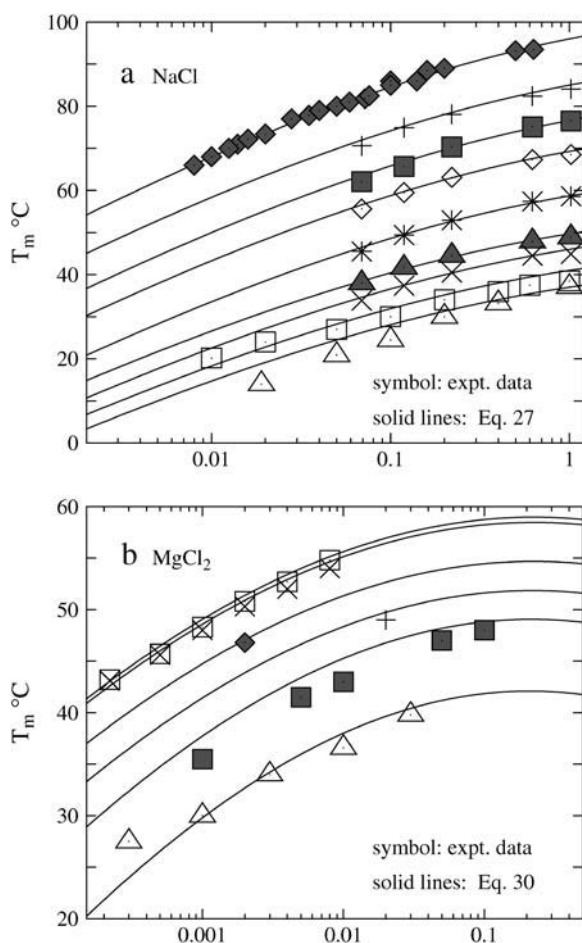
FIGURE 9   Comparisons between the empirical formulas (*solid lines*) for T_m (Eqs. 27 and 30) and experimental data (*symbols*) for (*a*) NaCl and (*b*) MgCl$_2$ solutions. (*a*) The DNA sequences for NaCl solutions are (5′-3′): GGAATTCC (81), GCCAGTTAA (37), ATCGTCTGGA (82), CCATTG-CTACC (35), ATCGTCTCGGTATAA (35), CCATCATTGTGTCTAC-CTCA (35), AATATCTCTCATGCGCCAAGCTACA (35), GTTATTCC-GCAGT-CCGATGGCAGCAGGCTC (35), and *E. coli* (33) (from the *bottom to top*). (*b*) The sequences for MgCl$_2$ solutions are (5′-3′): GCCAGTTAA (37), AGAAAGAGAAGA (84), TTTTTTTGTTTTTTT (38), TAATTTAAAATTTTTAAAAAA (88), TTTTTTTTTTTATTAAAA-TTTATAAA (89), and AAAAAAAAAAATAATTTTAAATATTT (89) (from the *bottom to top*). T_m(1 M Na$^+$) is calculated from the nearest neighbor model with the thermodynamic parameters of SantaLucia (20) except for *E. coli*. For *E. coli*, T_m(1 M Na$^+$) is taken as 96.5°C.

Nonadditivity for the helix stability

The analytical formulas for the thermodynamic parameters account for the chain length-dependence of the folding stability. The $1/N$ expansion clearly shows the saturation effect as $1/N \rightarrow 0$ for large helix length N (52).

The stability is additive if it can be computed as the sum of the stability of each base stack. Mathematically, the additivity corresponds to a linear-dependence of the folding free energy on the helix length (= $N - 1$ stacks), i.e., Δg_z in Eqs. 23 and 28 (z = valence of the ion = 1 for Na$^+$ and 2 for Mg^{2+}) is N-independent or weakly dependent on N, which,

according to Eqs. 24 and 31, occurs if the following condition is satisfied:

$$N^z \gg b_z/a_z,$$

where a_z and b_z are given by Eqs. 25 and 32 for $z = 1$ (Na$^+$) and 2 (Mg^{2+}), respectively.

The above additivity condition depends on the ion concentration. For example, b_z/a_z is not very sensitive to the ion concentration at high salt region ($\gtrsim 0.1$ M for NaCl and $\gtrsim 10$ mM for MgCl$_2$). But for lower ion concentration, the additivity condition becomes more sensitive to the ion concentration. b_z/a_z and hence the required chain length N would increase rapidly in order for the additivity condition to be satisfied.

Na$^+$ versus Mg^{2+}

Previous experiments for a specific sequence have shown that the 1 M NaCl solution has effectively the equivalent ionic effect on the helix stability as the 10 mM MgCl$_2$/150 mM NaCl mixed solution (36). Similar relation has also been experimentally found for RNA folding: 1 M NaCl has the similar effect as 10 mM MgCl$_2$/50 mM NaCl mixed solution for stabilizing a ribosomal RNA secondary structure (90), and 1 M NaCl is similar to 10 mM MgCl$_2$/100 mM NaCl mixed salt for a hammerhead ribozyme folding (91). With the TBI theory, which can treat the Mg^{2+} ions, we can now evaluate and compare the role of Na$^+$ and Mg^{2+} ion in the stabilization of nucleic acid helix. Because the current form of the TBI theory does not treat the Na$^+$/Mg^{2+} mixture solution, we examine the ds helix stability in 1 M NaCl and in 10 mM MgCl$_2$ solution. We compare the melting temperatures T_m in these two different solutions (see Eqs. 27 and 30).

We choose thermodynamic parameters of each base stack in 1 M NaCl ($\Delta H°$, $\Delta S°$) = (−8.36 kcal/mol, −22.37 cal/mol/K), as determined from the average parameters over different sequences (22). So for a N-bp helix, $\Delta H° \simeq -(N-1)8.36$ kcal/mol. Eqs. 27 and 30 predict that $\Delta T_m = T_m[1\,\text{M Na}^+] - T_M[10\,\text{mM Mg}^{2+}] \simeq 3.5°$ for $N = 9$. So the helix is only slightly less stable in 10 mM MgCl$_2$ than in 1 M NaCl.

In addition, we find that the melting temperature difference ΔT_m decreases as the helix length is increased and eventually becomes saturated for very long helix. Such length-dependence can be understood from the enthalpy-entropy competition in the ion-binding process. The ion-binding entropic penalty for [Mg^{2+}] = 10 mM is much larger than that for [Na$^+$] = 1 M. Therefore, entropically, Mg^{2+} binding is less favorable than Na$^+$ binding. However, enthalpically, the binding of Mg^{2+}, which carries higher charge and can cause more efficient charge neutralization, is more favorable than that of Na$^+$. Therefore, the enthalpic effect becomes more important for a longer helix, which has stronger electric field near DNA surface. As a result, as the helix length is increased, Mg^{2+} would stabilize the helix more effectively than Na$^+$, causing ΔT_m to decrease.

CONCLUSIONS AND DISCUSSION

The tightly bound ion theory can explicitly account for the correlation and fluctuation of the bound ions (55). Based on the TBI theory, we investigate the thermal stability of DNA helix in Na^+ and Mg^{2+} solutions for different helix lengths (5–13 bps) and different salt concentrations (1 mM to 1 M for NaCl and 0.1 mM to 1 M for $MgCl_2$). The predicted folding free energy and melting temperature for the helix-coil transition agree with the available experimental data. The following is a brief summary for our major findings in this study.

1. For NaCl solution, both PB and the TBI theory can successfully predict the thermodynamics of helix-coil transition up to 1 M NaCl, as compared with experimental data.
2. For $MgCl_2$, the TBI theory can predict the experimental data, whereas PB underestimates the helix stability and melting temperature due to the neglected correlation and fluctuation effects.
3. Helix is stabilized by ions. However, for high ion concentrations, the helix stability becomes saturated and further enhancement of the stability is small.
4. The electrostatic part of the helix-coil folding free energy appears only weakly temperature-dependent for both NaCl and $MgCl_2$ solutions. Thus, the strong temperature-dependence of the total folding free energy mainly comes from the nonelectrostatic contribution.
5. The nearest neighbor model works well for high NaCl concentration (and long helix), in which case the electrostatic part of the folding free energy for each base stack is only weakly dependent on the helix length N.
6. Based on our calculated results, we obtain analytical formulas for the folding free energy and the melting temperature as functions of helix length and salt concentration. These empirical formulas account for the non-additivity of the helix stability and are tested against extensive experimental results. These analytical expressions can be useful for practical use in predicting nucleic acid helix stability.

This work for the helix stability involves several simplified assumptions, as explained in the following. The stability calculation is based on the assumption about the separable electric and the nonelectric contributions. Moreover, the helix-coil transition is assumed to be two-state between the mean structures of dsDNA and ssDNA. However, ssDNA is a denatured structure that, depending on the sequence and ionic condition, can adopt an ensemble of different conformations. The uncertainty of the ssDNA structure may contribute to some of the theory-experiment differences.

In this form of the TBI theory, we do not treat: a), the mixed ion solutions, e.g., Na^+/Mg^{2+} mixture, and b), the possible existence of the anions in the tightly bound region.

The generalization of the current TBI framework to treat the mixed solution and the tightly bound anions is straightforward but technically challenging. Specifically, the multiple species (Na^+/Mg^{2+} or cation/anion) of the tightly bound ions can result in: 1), the significantly larger number of the binding modes, and 2), the much more complicated interactions and the associated potential of mean force functions.

In the TBI theory, we neglect the possible dehydration effect (92) for the bound ions. We also neglect the binding of ions (including anions) to specific functional groups of nucleotides (93) in the tightly bound region. The site-specific binding of dehydrated cations can contribute significantly to the nucleic acid tertiary structure folding stability. For the simple helical structure studied here, however, the binding to specific sites and the associated dehydration may not play a dominant role in the folding stability. Nevertheless, this TBI theory may provide a framework for further inclusion of the dehydration effects and ion binding to specific sites. A possible approach would be to place ion(s) to the predetermined specific binding site(s), and to determine the tightly bound region with the existence of the prefixed site-bound ion(s). To account for the desolvation effect for the tightly bound ions, we need to include the desolvation free energy ΔG_{sol} in the electrostatic free energy ΔG_b for the tightly bound ions.

To compute the stability for more complex nucleotide folds, we must consider the conformational ensemble of the molecule, including the possible stable intermediate states. For the high resolution full-atomic structure, the TBI calculation, in particular, the potential of mean force calculation for the tightly bound ions, would be more time-consuming because of the atomic details involved. Moreover, for a compact three-dimensional structure, different parts of the chain (and the associated tightly bound region) are brought together through the long-range tertiary contacts. As a result, a), the pairwise potential of mean force used in the helix-coil calculation should be replaced by the multiion potential of mean force to account for the correlation between the spatially nearby tightly bound ions, and b), in this case, the division of the tightly bound region into the tightly bound cells centered around the phosphates can become ambiguous.

APPENDIX A: STRUCTURAL MODELS FOR DSDNA AND SSDNA

We adopt B-DNA structure for dsDNA because B-form DNA is the most common and stable form over a wide range of salt conditions and sequences (16,94). The grooved primitive model is used instead of the all-atom DNA model (55,95); see Fig. 1 a. The model has been shown to be able to give detailed ion distribution that agrees well with the all-atomic simulations (95). In the grooved model, we represent a N-bp B-form DNA structure as two helical strands, each with N nucleotide units, around a central cylindrical rod of radius $r_{core} = 3.9$ Å. Two hard spheres are used to represent a nucleotide unit. A charged sphere with a point charge $-e$ at the center is used to represent the phosphate group and an electrically neutral sphere to represent the rest of the atoms. The phosphate sphere is placed at the center of the phosphate group of the nucleotide and the neutral sphere lies between the phosphate sphere and the cylindrical rod. Both spheres have radius of

$r_0 = 2.1$ Å (95). For a canonical B-DNA, the phosphate charge positions (= the center of the charged sphere) $(\rho_i^s, \theta_i^s, z_i^s)$ are given by the following equations (96): $\rho_i^s = 8.9(\text{Å})$; $\theta_i^s = \theta_0^s + i36°$; $z_i^s = z_0^s + i3.4(\text{Å})$, where $s = 1$, 2 denotes the two strands and $i = 1, 2, \ldots N$ denotes the nucleotides on each strand. The parameters (θ_0^s, z_0^s) for the initial position are $(0°, 0 \text{ Å})$ for the first strand and $(154.4°, 0.78 \text{ Å})$ for the second strand, respectively.

The ssDNA structure is not as well-characterized as the dsDNA. The structure of ssDNA, which is an ''unfolded'' state of the dsDNA, can be dependent on the helix and the ionic condition (94,97–103). Previous experiments indicated that ssDNA (RNA) structure is neither a maximally stretched ''rod'' nor a completely random conformation. Instead, the ssDNA structure exhibits some single helical order due to self-stacking (94,97–103). This suggests that the single-strand structure can be modeled as an ordered helix (58,60). In this work, instead of considering the ensemble of all ssDNA conformations (104), we model ssDNA using a mean structure averaged over the previously measured ssDNA structures (32,58,60,100–102). We use the grooved primitive (55,95) model to describe the ssDNA structure; see Fig. 1 b. There are three structure parameters to be determined: radial coordinate of phosphates r_p, twist angle per residue $\Delta\theta$, and rise per basepair Δz. The experiments show that, compared with dsDNA, the single-stranded helices shrink (i.e., r_p and Δz decrease) because of the absence of the interstrand electrostatic repulsion (94,97–99). Previous theoretical modeling on ssDNA structure suggests that the radial radius of phosphate charges (r_p) is between 5 and 7 Å (32,58,60,100–102). Here, we use $r_p = 7$ Å We also use $\Delta z = 2.2$Å and keep $\Delta\theta = 36°$, which is the same as that of dsDNA. Thus, for ssDNA, the phosphate charge position (ρ_i, θ_i, z_i) can be given by the following equations: $\rho_i = 7$ (Å); $\theta_i = i\,36°$; $z_i = i\,2.2$ (Å). As a control, we also perform calculations with the other two different sets of structure parameters for ssDNA: $(\Delta\theta, r_p, \Delta z) = (36°, 7.5 \text{ Å}, 1.8 \text{ Å})$ and $(\Delta\theta, r_p, \Delta z) = (36°, 6.4 \text{ Å}, 2.6 \text{ Å})$ and found negligible changes in the predicted results for both NaCl and MgCl$_2$ solutions.

APPENDIX B: PARAMETER SETS AND NUMERICAL DETAILS

In this study, the ions are assumed to be hydrated (55). The radii of hydrated Na$^+$ and Mg^{2+} ions are taken as 3.5 and 4.5 Å (105), respectively. In addition, the cation sizes can be changed (3, 3.5, and 4 Å for monovalent and 4, 4.5, and 5 Å for divalent ions) to investigate the cation size effects on the DNA stability.

In the computation with PB, the dielectric constant ϵ of DNA interior is set to be 2, and ϵ of solvent is set as the value of bulk water. At 25°C, the dielectric constant of water is $\sim$78. The dielectric constant of water decreases with the increase of temperature. We use the following empirical formula for the temperature-dependence of ϵ (86)

$$\epsilon(t) = 87.740 - 0.4008 \times t + 9.398 \times 10^{-4} \times t^2 - 1.41 \times 10^{-6} \times t^3, \qquad (33)$$

where t is the temperature in Celsius.

Both the TBI model and the PB calculation require numerical solution of the nonlinear PB. We have developed a three-dimensional finite-difference algorithm to numerically solve nonlinear PB equation (55), by following the existed algorithms (44–51). A thin layer of thickness equal to one cation radius is added to the molecular surface to account for the excluded volume layer of cations (8,9,55). We use the three-step focusing process to obtain the detailed ion distribution near the molecules (45,55). The grid size of the first run depends on the salt concentration used. Generally, we keep it larger than six times of Debye length of salt solution to include all salt effects in solution. The resolution of the first run varies with the grid size to make the iterative process viable within a reasonable computational time (55). The grid sizes for the second run and the third run are kept at 102 and 51 Å, respectively, and the corresponding resolutions are 0.85 Å per grid and 0.425 Å per grid, respectively. Then the number of the grid points is 121^3 for the second and third run. We use high resolution grid system near the DNA

surface because the ions near the DNA surface make the most important electrostatic contribution to DNA stability. We have examined our results against different grid sizes, and the results are quite stable.

REFERENCES

1. Tinoco, I., and C. Bustamante. 1999. How RNA folds. *J. Mol. Biol.* 293:271–281.

2. Rook, M. S., D. K. Treiber, and J. R. Williamson. 1999. An optimal Mg^{2+} concentration for kinetic folding of the Tetrahymena ribozyme. *Proc. Natl. Acad. Sci. USA.* 96:12471–12476.

3. Woodson, S. A. 2005. Metal ions and RNA folding: a highly charged topic with a dynamic future. *Curr. Opin. Chem. Biol.* 9:104–109.

4. Draper, D. E., D. Grilley, and A. M. Soto. 2005. Ions and RNA folding. *Annu. Rev. Biophys. Biomol. Struct.* 34:221–243.

5. Sosnick, T. R., and T. Pan. 2003. RNA folding: models and perspectives. *Curr. Opin. Struct. Biol.* 13:309–316.

6. Auffinger, P., L. Bielecki, and E. Westhof. 2004. Symmetric K$^+$ and Mg^{2+} ion-binding sites in the 5S rRNA loop E inferred from molecular dynamics simulations. *J. Mol. Biol.* 335:555–571.

7. Auffinger, P., and E. Westhof. 2001. Water and ion binding around r(UpA)$_{12}$ and d(TpA)$_{12}$ oligomers: comparison with RNA and DNA (CpG)$_{12}$ duplexes. *J. Mol. Biol.* 305:1057–1072.

8. Misra, V. K., and D. E. Draper. 2000. Mg^{2+} binding to tRNA revisited: the nonlinear Poisson-Boltzmann model. *J. Mol. Biol.* 299:813–825.

9. Misra, V. K., and D. E. Draper. 2001. A thermodynamic framework for Mg^{2+} binding to RNA. *Proc. Natl. Acad. Sci. USA.* 98:12456–12461.

10. Heilman-Miller, S. L., D. Thirumalai, and S. A. Woodson. 2001. Role of counterion condensation in folding of the Tetrahymena ribozyme. I. Equilibrium stabilization by cations. *J. Mol. Biol.* 306:1157–1166.

11. Heilman-Miller, S. L., J. Pan, D. Thirumalai, and S. A. Woodson. 2001. Role of counterion condensation in folding of the Tetrahymena ribozyme. II. Counterion-dependence of folding kinetics. *J. Mol. Biol.* 309:57–68.

12. Das, R., L. W. Kwok, I. S. Millett, Y. Bai, T. T. Mills, J. Jacob, G. S. Maskel, S. Seifert, S. G. J. Mochrie, P. Thiyagarajan, S. Doniach, L. Pollack, et al. 2003. The fastest global events in RNA folding: electrostatic relaxation and tertiary collapse of the Tetrahymena ribozyme. *J. Mol. Biol.* 332:311–319.

13. Koculi, E., N. K. Lee, D. Thirumalai, and S. A. Woodson. 2004. Folding of the Tetrahymena ribozyme by polyamines: importance of counterion valence and size. *J. Mol. Biol.* 341:27–36.

14. Fang, X., T. Pan, and T. R. Sosnick. 1999. A thermodynamic framework and cooperativity in the tertiary folding of a Mg^{2+}-dependent ribozyme. *Biochemistry.* 38:16840–16846.

15. Bloomfield, V. A. 1997. DNA condensation by multivalent cations. *Biopolymers.* 44:269–282.

16. Bloomfield, V. A., D. M. Crothers, and I. Tinoco Jr. 2000. Nucleic Acids: Structure, Properties and Functions. University Science Books, Sausalito, CA.

17. Freier, S. M., R. Kierzek, J. A. Jaeger, N. Sugimoto, M. H. Caruthers, T. Neilson, and D. H. Turner. 1986. Improved free-energy parameters for predictions of RNA duplex stability. *Proc. Natl. Acad. Sci. USA.* 83:9373–9377.

18. Breslauer, K. J., R. Frank, H. Blocker, and L. A. Marky. 1986. Predicting DNA duplex stability from the base sequence. *Proc. Natl. Acad. Sci. USA.* 83:3746–3750.

19. Turner, D. H., and N. Sugimoto. 1988. RNA structure prediction. *Annu. Rev. Biophys. Biophys. Chem.* 17:167–192.

20. SantaLucia, J., H. T. Allawi, and P. A. Seneviratne. 1996. Improved nearest-neighbor parameters for predicting DNA duplex stability. *Biochemistry.* 35:3555–3562.

21. Sugimoto, N., S. I. Nakano, M. Yoneyama, and K. I. Honda. 1996. Improved thermodynamic parameters and helix initiation factor to predict stability of DNA duplexes. *Nucleic Acids Res.* 24:4501–4505.

22. SantaLucia, J., Jr. 1998. A unified view of polymer, dumbbell, and oligonucleotide DNA nearest-neighbor thermodynamics. *Proc. Natl. Acad. Sci. USA.* 95:1460–1465.

23. Owczarzy, R., P. M. Callone, F. J. Gallo, T. M. Paner, M. J. Lane, and A. S. Benight. 1997. Predicting sequence-dependent melting stability of short duplex DNA oligomers. *Biopolymers.* 44:217–239.

24. Elson, E. L., I. E. Scheffler, and R. L. Baldwin. 1970. Helix formation by (TA) oligomers. III. Electrostatic effects. *J. Mol. Biol.* 54:401–415.

25. Record, M. T., Jr. 1975. Effects of Na^+ and Mg^{2+} ions on the helix-coil transition of DNA. *Biopolymers.* 14:2137–2158.

26. Patel, D. J., S. A. Kozlowski, L. A. Marky, C. Broka, J. A. Rice, K. Itakura, and K. J. Breslauer. 1982. Premelting and melting transition in the d(CGCGAATTCGCG) self-complementary duplex in solution. *Biochemistry.* 21:428–436.

27. Hickey, D. R., and D. H. Turner. 1985. Solvent effects on the stability of A_7U_7p. *Biochemistry.* 24:2086–2094.

28. Erie, D., N. Sinha, W. Olson, R. Jones, and K. Breslauer. 1987. A dumbbell-shaped, double-hairpin structure of DNA: a thermodynamic investigation. *Biochemistry.* 26:7150–7159.

29. Delcourt, S. G., and R. D. Blake. 1991. Stacking energies in DNA. *J. Biol. Chem.* 266:15160–15169.

30. Anderson, C. F., and T. M. Record. 1995. Salt-nucleic acid interactions. *Annu. Rev. Phys. Chem.* 46:657–700.

31. Rentzeperis, D., J. Ho, and L. A. Marky. 1993. Contribution of loops and nicks to the formation of DNA dumbbells: melting behavior and ligand binding. *Biochemistry.* 32:2564–2572.

32. Shkel, I., and M. T. Record. 2004. Effect of the number of nucleic acid oligomer charges on the salt dependence of stability (ΔG°_{37}) and melting temperature (T_m): NLPB analysis of experimental data. *Biochemistry.* 43:7090–7101.

33. Schildkraut, C., and S. Lifson. 1965. Dependence of the melting temperature of DNA on salt concentration. *Biopolymers.* 3:195–208.

34. Blake, R. D., and S. G. Delcourt. 1998. Thermal stability of DNA. *Nucleic Acids Res.* 26:3323–3332.

35. Owczarzy, R., Y. You, B. G. Moreira, J. A. Manthey, L. Huang, M. A. Behlke, and J. A. Walder. 2004. Effects of sodium ions on DNA duplex oligomers: improved predictions of melting temperatures. *Biochemistry.* 43:3537–3554.

36. Williams, A. P., C. E. Longfellow, S. M. Freier, R. Kierzek, and D. H. Turner. 1989. Laser temperature-jump, spectroscopic, and thermodynamic study of salt effects on duplex formation by dGCATGC. *Biochemistry.* 28:4283–4291.

37. Nakano, S., M. Fujimoto, H. Hara, and N. Sugimoto. 1999. Nucleic acid duplex stability: influence of base composition on cation effects. *Nucleic Acids Res.* 27:2957–2965.

38. Hou, M. H., S. B. Lin, J. M. Yuann, W. C. Lin, A. H. J. Wang, and L. S. Kan. 2001. Effects of polyamines on the thermal stability and formation kinetics of DNA duplex with abnormal structure. *Nucleic Acids Res.* 29:5121–5128.

39. Serra, M. J., J. D. Baird, T. Dale, B. L. Fey, K. Retatagos, and E. Westhof. 2002. Effects of magnesium ions on the stabilization of RNA oligomers of defined structures. *RNA.* 8:307–323.

40. SantaLucia, J., Jr., and D. Hicks. 2004. The thermodynamics of DNA structural motifs. *Annu. Rev. Biophys. Biomol. Struct.* 33:415–440.

41. Manning, G. S. 1978. The molecular theory of polyelectrolyte solutions with applications to the electrostatic properties of polynucleotides. *Q. Rev. Biophys.* 11:179–246.

42. Oosawa, F. 1971. Polyelectrolytes. Marcel Dekker, New York.

43. Manning, G. S. 2001. Counterion condensation on a helical charge lattice. *Macromolecules.* 34:4650–4655.

44. Klapper, I., R. Hagstrom, R. Fine, K. Sharp, and B. Honig. 1986. Focusing of electric fields in the active site of Cu-Zn superoxide dismutase: effects of ionic strength and amino-acid modification. *Proteins.* 1:47–59.

45. Gilson, M. K., K. A. Sharp, and B. Honig. 1987. Calculating the electrostatic potential of molecules in solution: method and error assessment. *J. Comput. Chem.* 9:327–335.

46. Sharp, K. A., and B. Honig. 1990. Calculating total electrostatic energies with the nonlinear Poisson-Boltzmann equation. *J. Phys. Chem.* 94:7684–7692.

47. Nicholls, A., and B. Honig. 1991. A rapid finite-difference algorithm, utilizing successive over-relaxation to solve the Poisson-Boltzmann equation. *J. Comput. Chem.* 12:435–445.

48. You, T. J., and S. C. Harvey. 1993. Finite element approach to the electrostatics of macromolecules with arbitrary geometries. *J. Comput. Chem.* 14:484–501.

49. Baker, N. A., D. Sept, S. Joseph, M. J. Holst, and J. A. McCammon. 2000. Electrostatics of nanosystems: application to microtubules and the ribosome. *Proc. Natl. Acad. Sci. USA.* 98:10037–10041.

50. Grant, J. A., B. T. Pickup, and A. Nicholls. 2001. A smooth permittivity function for Poisson-Boltzmann solvation methods. *J. Comput. Chem.* 22:608–640.

51. Sept, D., N. A. Baker, and J. A. McCammon. 2003. The physical basis of microtubule structure and stability. *Protein Sci.* 12:2257–2261.

52. Record, M. T., Jr., and T. M. Lohman. 1978. A semiempirical extension of polyelectrolyte theory to the treatment of oligoelectrolytes: application to oligonucleotide helix-coil transitions. *Biopolymers.* 17:159–166.

53. Fenley, M. O., G. S. Manning, and W. K. Olson. 1990. Approach to the limit of counterion condensation. *Biopolymers.* 30:1191–1203.

54. Manning, G. S., and U. Mohanty. 1997. Counterion condensation on ionic oligomers. *Physica A.* 247:196–204.

55. Tan, Z. J., and S. J. Chen. 2005. Electrostatic correlations and fluctuations for ion binding to a finite length polyelectrolyte. *J. Chem. Phys.* 122:044903.

56. Kotin, L. 1963. On the effect of ionic strength on the melting temperature of DNA. *J. Mol. Biol.* 7:309–311.

57. Baldwin, R. L. 1971. Experimental tests of the theory of deoxyribonucleic acid melting with d(T-A) oligomers. *Acc. Chem. Res.* 4:265–272.

58. Korolev, N., A. P. Lyubartsev, and L. Nordenskiöld. 1998. Application of polyelectrolyte theories for analysis of DNA melting in the presence of Na^+ and Mg^{2+} ions. *Biophys. J.* 75:3041–3056.

59. Friedman, R. A., and B. Honig. 1995. A free energy analysis of nucleic acid base stacking in aqueous solution. *Biophys. J.* 69:1528–1535.

60. Korolev, N., A. P. Lyubartsev, and L. Nordenskiöld. 2002. Application of the Poisson-Boltzmann polyelectrolyte model for analysis of thermal denaturation of DNA melting in the presence of Na^+ and polyamine cations. *Biophys. Chem.* 104:55–66.

61. Xia, T., J. SantaLucia, M. E. Burkard, R. Kierzek, S. J. Schroeder, X. Jiao, C. Cox, and D. H. Turner. 1998. Thermodynamic parameters for an expanded nearest-neighbor model for formation of RNA duplexes with Watson-Crick base pairs. *Biochemistry.* 37:14719–14735.

62. Holbrook, J. A., M. W. Capp, R. M. Saecker, and M. T. Record, Jr. 1999. Enthalpy and heat capacity changes for formation of an oligomeric DNA duplex: interpretation in terms of coupled processes of formation and association of single-stranded helices. *Biochemistry.* 38:8409–8422.

63. Takach, J. C., P. J. Mikulecky, and A. L. Feig. 2004. Salt-dependent heat capacity changes for RNA duplex formation. *J. Am. Chem. Soc.* 126:6530–6531.

64. Petruska, J., and M. F. Goodman. 1995. Enthalpy-entropy compensation in DNA melting thermodynamics. *J. Biol. Chem.* 270:746–750.

65. Rouzina, I., and V. A. Bloomfield. 1999. Heat capacity effects on the melting of DNA. 1. General aspects. *Biophys. J.* 77:3242–3251.

66. Rouzina, I., and V. A. Bloomfield. 1999. Heat capacity effects on the melting of DNA. 2. Analysis of nearest-neighbor base pair effects. *Biophys. J.* 77:3252–3255.

67. Wu, P., S. I. Nakano, and N. Sugimoto. 2002. Temperature dependence of thermodynamic properties for DNA/DNA and RNA/DNA duplex formation. *Eur. J. Biochem.* 269:2821–2830.

68. SantaLucia, J., Jr., and D. H. Turner. 1998. Measuring the thermodynamics of RNA secondary structure formation. *Biopolymers.* 44:309–319.

69. Rouzina, I., and V. A. Bloomfield. 1996. Macroion attraction due to electrostatic correlation between screening counterions.1. Mobile surface-adsorbed ions and diffuse ion cloud. *J. Phys. Chem.* 100:9977–9989.

70. Pollock, E., and J. Hansen. 1973. Statistical mechanics of dense ionized matter. II. Equilibrium properties and melting transition of the crystallized one-component plasma. *Phys. Rev. A.* 8:3110–3122.

71. Slattery, W., G. Doolen, and H. Dewitt. 1980. Improved equation of state for the classical one-component plasma. *Phys. Rev. A.* 21:2087–2095.

72. Ichimaru, S., H. Iyetomi, and S. Tanaka. 1987. Statistical physics of dense plasmas: thermodynamics, transport coefficients and dynamic correlations. *Phys. Rep.* 149:91–205.

73. Lindemann, F. A. 1910. The calculation of molecular vibration frequencies. *Z. Phys.* 11:609–612.

74. Zhou, Y., M. Karplus, K. D. Ball, and R. S. Berry. 2002. The distance fluctuation criterion for melting: comparison of square-well and Morse potential models for clusters and homopolymers. *J. Chem. Phys.* 116:2323–2329.

75. Truskett, T. M., S. Torquato, S. Sastry, P. G. Debenedetti, and F. H. Stillinger. 1998. Structural precursor to freezing in the hard-disk and hard sphere systems. *Phys. Rev. E.* 58:3083–3088.

76. Overbeek, J. Th. G. 1990. The role of energy and entropy in the electrical double layer. *Colloids Surf.* 51:61–75.

77. Stigter, D. 1995. Evaluation of the counterion condensation theory of polyelectrolytes. *Biophys. J.* 69:380–388.

78. Vyazovkina, E. V., E. V. Savchenko, S. G. Lokhov, J. W. Engels, E. Wickstrom, and A. V. Lebedev. 1994. Synthesis of specific diastereomers of a DNA methylphosphonate heptamer, d(CpCpApApApC-pA), and stability of base pairing with the normal DNA octamer d(TpGpTpTpTpGpGpC). *Nucleic Acids Res.* 22:2404–2409.

79. Braunlin, W. H., and V. A. Bloomfield. 1991. ^{1}H NMR study of the base pairing reaction of the d(GGAATTCC): salt effects on the equilibria and kinetics of strand association. *Biochemistry.* 30:754–758.

80. Patel, D. J., and L. L. Canuel. 1979. Helix-coil transition of the self-complementary dG-dG-dA-dA-dT-dT-dC-dC duplex. *Eur. J. Biochem.* 96:267–276.

81. Bower, M., M. F. Summers, B. Kell, J. Hoskins, G. Zon, and W. D. Wilson. 1987. Synthesis and characterization of oligodeoxyribonucleotides containing terminal phosphates. NMR, UV spectroscopic and thermodynamic analysis of duplex formation of [d(pGGAATTCC)]$_2$, [d(GGAATTCCp)]$_2$, and [d(pGGAATTCCp)]$_2$. *Nucleic Acids Res.* 15:3531–3547.

82. Owczarzy, R., I. Dunietz, M. A. Behlke, I. M. Klotz, and J. A. Walder. 2003. Thermodynamic treatment of oligonucleotide duplex-simplex equilibria. *Proc. Natl. Acad. Sci. USA.* 100:14840–14845.

83. Soto, A. M., W. H. Gmeiner, and L. A. Marky. 2002. Energetic and conformational contributions to the stability of Okazaki fragments. *Biochemistry.* 41:6842–6849.

84. Sugimoto, N., P. Wu, H. Hara, and Y. Kawamoto. 2001. pH and cation effects on the properties of parallel pyrimidine motif DNA triplexes. *Biochemistry.* 40:9396–9405.

85. Wu, P., Y. Kawamoto, H. Hara, and N. Sugimoto. 2002. Effect of divalent cations and cytosine protonation of thermodynamic properties of intermolecular DNA double and triple helices. *J. Inorg. Biochem.* 91:277–285.

86. Eisenberg, D., and W. Kauzmann. 1969. The Structure and Properties of Water. Oxford University Press, Oxford, UK.

87. von Ahsen, N., M. Oellerich, V. W. Armstrong, and E. Schutz. 1999. Application of a thermodynamic nearest-neighbor model to estimate nucleic acid stability and optimize probe design: prediction of melting points of multiple mutations of apolipoprotein B-3500 and factor V with a hybridization probe genotyping assay on the lightcycle. *Clin. Chem.* 45:2094–2101.

88. Ramsing, N. B., K. Rippe, and T. M. Jovin. 1989. Helix-coil transition of parallel-stranded DNA. Thermodynamics of hairpin and linear duplex oligonucleotides. *Biochemistry.* 28:9528–9535.

89. Rippe, K., N. B. Ramsing, and T. M. Jovin. 1989. Spectroscopic properties and helical stabilities of 25-nt parallel-stranded linear DNA duplexes. *Biochemistry.* 28:9536–9541.

90. Jaeger, J. A., M. Zuker, and D. H. Turner. 1990. Melting and chemical modification of a cyclized self-splicing group I intron: similarity of structures in 1 M Na$^+$, in 10 mM Mg^{2+}, and in the presence of substrate. *Biochemistry.* 29:10147–10158.

91. Mikulecky, P. J., J. C. Takach, and A. L. Feig. 2004. Entropy-driven folding of an RNA helical junction: an isothermal titration calorimetric analysis of the hammerhead ribozyme. *Biochemistry.* 43:5870–5881.

92. Misra, V. K., and D. E. Draper. 1998. On the role of magnesium ions in RNA stability. *Biopolymers.* 48:113–135.

93. Auffinger, P., L. Bielecki, and E. Westhof. 2004. Anion binding to nucleic acids. *Structure.* 12:379–388.

94. Saenger, W. 1984. Principles of Nucleic Acid Structure. Springer-Verlag, New York.

95. Montoro, J. C. G., and J. L. F. Abascal. 1995. Ionic distribution around simple DNA models. I. Cylindrically averaged properties. *J. Chem. Phys.* 103:8273–8284.

96. Arnott, S., and D. W. L. Hukins. 1972. Optimised parameters for A-DNA and B-DNA double-helices. *Biochem. Biophys. Res. Commun.* 47:1504–1509.

97. Suck, D., P. C. Manor, and W. Saenger. 1976. The structure of a trinucleoside diphosphate: adenylyl-(3′,5′)-adenylyl(3′,5′)-adenosine hexahydrate. *Acta Crystallogr. B.* 32:1727–1737.

98. Arnott, S., R. Chandrasekaran, and A. G. W. Leslie. 1976. Structure of the single-stranded polyribonucleotide polycytidylic acid. *J. Mol. Biol.* 106:735–748.

99. Camerman, N., J. K. Fawcett, and A. Camerman. 1976. Molecular structure of a deoxyribose-dinucleotide, sodium thymidylyl-(5′ yields to 3′)-thymidylate-(5′) hydrate (pTpT), and a possible structural model for polythymidylate. *J. Mol. Biol.* 107:601–621.

100. Olmsted, M. C., C. F. Anderson, and M. T. Record, Jr. 1991. Importance of oligoelectrolyte end effects for the thermodynamics of conformational transitions of nucleic acid oligomers: a grand canonical Monte Carlo analysis. *Biopolymers.* 31:1593–1604.

101. Duguid, J. G., and V. A. Bloomfield. 1996. Electrostatic effects on the stability of condensed DNA in the presence of divalent cations. *Biophys. J.* 70:2838–2846.

102. Trend, B. L., D. A. Knoll, M. Ueno, D. F. Evans, and V. A. Bloomfield. 1990. Cation radius effects on the helix-coil transition of DNA. *Biophys. J.* 57:829–834.

103. Vesnaver, G., and K. J. Breslauer. 1991. The contribution of DNA single-stranded order to the thermodynamics of duplex formation. *Proc. Natl. Acad. Sci. USA.* 88:3569–3573.

104. Dimitrov, R. A., and M. Zuker. 2004. Prediction of hybridization and melting for double-stranded nucleic acids. *Biophys. J.* 87:215–226.

105. Marcus, Y. 1985. Ion Solvation. John Wiley & Sons, Chichester, UK.